TD-15-007
June 25, 2015

Invited paper for a special issue of the IEEE Transactions on Nuclear Science (TNS) in commemoration of the 50th anniversary of the original Particle Accelerator Conference (FERMILAB-PUB-15-274-TD)

Research and Development of Nb_3Sn Wires and Cables for High-Field Accelerator Magnets

Emanuela Barzi, Alexander V. Zlobin
Fermi National Accelerator Laboratory (FNAL)
Pine and Kirk Rds, Batavia, IL 60510, U.S.
E-mail: barzi@fnal.gov

***Abstract*– The latest strategic plans for High Energy Physics endorse a continued world leadership role in superconducting magnet technology for future Energy Frontier Programs. This includes 10 to 15 T Nb_3Sn accelerator magnets for LHC upgrades and eventually for a future 100 TeV scale proton-proton collider. This paper describes the multi-decade R&D investment in the Nb_3Sn superconductor technology, which was crucial to produce the first reproducible 10 to 12 T accelerator-quality dipoles and quadrupoles, as well as their scale-up. We also indicate prospective research areas in superconducting Nb_3Sn wires and cables to achieve the next goals for superconducting accelerator magnets. Emphasis is on increasing performance and decreasing costs while pushing the Nb_3Sn technology to its limits of 15 to 16 T field for future pp colliders.**

I. Introduction and Historical Overview

Superconducting materials have found a wide range of applications in science and society. Superconducting magnets and radio frequency (SRF) structures are at the heart of most particle accelerators for fundamental science, as well as accelerators for medical isotope production and ion therapy treatment.

For a circular collider of given size, its energy is limited by the strength of the bending dipole magnets. Moreover, for both linear and circular machines, their maximum luminosity is determined, among other factors, by the strength of quadrupole magnets used for the final beam focusing. That is why there has been enduring interest in the High Energy Physics (HEP) and Particle Accelerator communities in higher-field and higher-gradient accelerator magnets. The highest fields have been achieved using superconducting electromagnets, but the maximum nominal field of NbTi accelerator magnets used in all present high-energy machines, including the Large Hadron Collider (LHC) at the European Organization for Nuclear Research (CERN, Switzerland), is limited to ~8 T at an operating temperature of 1.9 K.

To push the magnetic field in accelerator magnets beyond the NbTi LHC magnets, superconductors with higher critical parameters are needed. Among the many known high-field superconductors only Nb_3Sn, Nb_3Al, BSCCO ($Bi_2Sr_2CaCu_2O_8$ or $Bi_2Sr_2Ca_2Cu_3O_{10}$) and REBCO ($REBa_2Cu_3O_7$, where RE stands for rare earth element) are sufficiently developed to be presently used in magnets above 10 T. These superconductors are industrially produced in the form of composite materials in long (~1 km) length, as required for accelerator magnets.

The intermetallic compound Nb_3Sn is a type II superconductor having a well-defined stoichiometry and the A15 crystal structure. It has a critical temperature T_{c0} of up to 18.3 K and an upper critical magnetic field B_{c20} of up to 30 T [1]. As a comparison, the ductile alloy NbTi has a T_{c0} of 9.3 K and a B_{c20} of 15 T. Thanks to Nb_3Sn stronger superconducting properties, it enables magnets above 10 T. At a world production of 400+ tons/year, it is the second superconducting material most widely used in large-scale magnet applications. For instance, it is the material of choice for Nuclear Magnetic Resonance (NMR) spectrometers, which have become a key

Work supported by Fermi Research Alliance, LLC, under contract No. DE-AC02-07CH11359 with the U.S. Department of Energy.

analysis tool in modern biomedicine, chemistry and materials science. These systems use fields up to 23.5 T, which correspond to a Larmor frequency of 1000 MHz. Nb_3Sn is also used in high field magnets for the plasma confinement in fusion reactors. The International Thermonuclear Fusion Research and Engineering project (ITER, France) includes a Central Solenoid of 13.5 T. Some of the challenges are that Nb_3Sn requires high-temperature processing, which makes it brittle, and its critical current is strain sensitive, i.e. high strain on the sample may reduce or totally destroy its superconductivity.

The A15 crystal structure was first discovered in 1953 by Hardy and Hulm in V_3Si, which has a T_{c0} of 17 K [2]. A year later, Matthias et al. discovered Nb_3Sn [3]. The first laboratory attempt to produce wires was in 1961 by Kunzler et al. [4] by filling Nb tubes with crushed powders of Nb and Sn. The tube was sealed, compacted, and drawn to long wires. This primitive Powder-in-Tube (PIT) technique required reaction at high temperature, in the range of 1000 to 1400ºC, to form the superconducting phase. Nevertheless, that same year it was used to fabricate the first 6 T magnet. An initial alternative to the PIT and the first commercial production was in 1967 in the form of tapes by surface diffusion process. Benz and Coffin passed a Nb tape through a bath of molten Sn, and reacted the coated tape to form Nb_3Sn. Although successful in demonstrating the use of Nb_3Sn in high-field magnets, neither technique was practical. The large filaments in the case of the PIT wire, and the inherently large aspect ratio of the tape, invariably resulted in large trapped magnetization and flux jump instabilities. In the late 1960s, Tachikawa introduced an alternative concept based on solid state diffusion [5]. This principle has been used to fabricate Nb_3Sn wires by the so-called bronze route [6-7], which is today one of the leading techniques for manufacturing Nb_3Sn.

In the 1980s and 90s conductor development programs for accelerator magnets were focused on NbTi composite wires and were driven by the needs of accelerators such as the Tevatron, UNK, SSC and LHC. The development of Nb_3Sn conductor at that time was mainly steered by fusion magnet programs [8]. It is since the late 1990s that the HEP community has taken leadership in the development of Nb_3Sn wires for post-LHC accelerators, and used these wires for high field accelerator magnets R&D, which has led to magnetic fields beyond the limits of NbTi technology. Among the several manufacturing processes that have been developed to produce superconducting Nb_3Sn wires in addition to the bronze route, there is the Internal Tin (IT) technique, which includes as variants the Modified Jelly Roll (MJR) and the Restacked Rod processes (RRP®) [9] by Oxford Instruments – Superconducting Technology (OST), as well as a more sophisticated PIT method [10]. Nb_3Sn properties and fabrication methods are reviewed elsewhere [9-14].

Accelerator magnets need high-current multi-strand superconducting cables to reduce the number of turns in the coils, and thus magnet inductance. In addition using multi-strand cables allows limiting the piece length requirement for wire manufacturing which is important for large magnets. To achieve in a cable the required current, several strands have to be connected in parallel and twisted or transposed in the axial direction. The strands in a cable are not insulated from each other to allow current redistribution between strands in the case of localized defects or quenches. There are several different types of cable used in accelerator magnets [15]. The Rutherford cable, developed at the Rutherford Appleton Laboratory (RAL) [16], has played a crucial role in establishing NbTi accelerator magnet technology. It is widely used in modern high energy accelerators and colliders thanks to its excellent mechanical, electrical and thermal properties. Superconducting dipoles and quadrupoles based on this cable design and on NbTi strands were successfully used in the Tevatron, HERA, RHIC and LHC [15]. A new generation of accelerator magnets, being developed in the US [17] and in Europe [18] is using Rutherford-type cables based on Nb_3Sn strands.

The next section II of this paper, "Nb_3Sn Composite Wires", briefly describes the existing Nb_3Sn wire technologies and then focuses on identifying parameters that are important for accelerator magnet design and operation. Past and present R&D programs are touched on, as well as Nb_3Sn wire state-of-the-art performance. The following section III on "Nb_3Sn Wire Properties" details those key research activities and methods used in the International community that helped study and solve most of the aspects required of Nb_3Sn wires for magnet realization. The next two sections IV and V on "Nb_3Sn Rutherford Cables" and "Nb_3Sn Rutherford Cable Properties" attempt to do the same for cables, and finally in the "Next Steps and R&D Goals" section we discuss important research topics for Nb_3Sn to help achieve 15 to 16 T accelerator magnet field and cost reduction goals.

II. Nb_3Sn Composite Wires

Requirements of superconductor stability with respect to magnetic flux jumps and superconductor protection in case of transition to the normal state led to the concept of composite superconducting wire, in which thin superconducting filaments are distributed in a normal low resistance matrix [19]. This matrix provides several important functions. It conducts heat away from the surface of the superconducting filaments thanks to high thermal conductivity, absorbs a substantial fraction of heat due to high specific heat, and decreases Joule heating when the superconductor becomes normal. To reduce the eddy currents induced by varying external fields and improve stability of a composite wire to flux jumps, these filaments are twisted along the conductor axis.

In this section, we briefly touch on Nb_3Sn wire technologies, describe the heat treatment cycle and its functions, identify fundamental parameters and properties of Nb_3Sn wires, summarize the most recent conductor R&D programs, and describe commercial wires and their progress.

A. Nb_3Sn Composite Wire Fabrication

Nb_3Sn composite wires are currently produced using three main methods: bronze, internal tin, and powder-in-tube [14]. Important features of practical materials for superconducting accelerator magnets include performance and its reproducibility in long lengths, commercial production and affordable cost.

The bronze process (Br) is based on a large number of Nb

filaments dispersed in a Sn-rich bronze matrix. The initial billet is made of hundreds of Nb rods and it is drawn into a hexagonal element of intermediate size. The rods are then cut and assembled in a second billet, which is extruded, annealed and drawn to final wire size. The bronze core is surrounded by a high-purity Cu matrix which is separated by a thin Nb or Ta diffusion barrier. The bronze route provides the smallest filament size (~2-3 μm), but has a relatively low J_c due to the limited Sn content in bronze.

The Internal Tin (IT) process was introduced in 1974 by Hashimoto et al. [20] to overcome the limits of the Br method. It is based on assembling a large number of Nb filaments and pure Sn or Sn-alloy rods in a Cu matrix. The assembly is surrounded by a thin Nb or Ta barrier to prevent Sn diffusion into the high-purity Cu matrix, and it is then extruded and drawn down to final size. Restacking of assemblies allows reducing the final subelement size. Due to the optimal amount of Sn this process gives the highest J_c, but limits the minimal subelement size attainable in the final wire.

The Powder-in-Tube (PIT) process is based on stacking thick-wall Nb tubes, filled with fine $NbSn_2$ powder in a high-purity Cu matrix. The stacked assembly is drawn or extruded to final wire size. This method allows an optimal combination of small filament size (<50 μm) and high J_c comparable with the IT process. However, the cost of PIT wire is 2 to 3 times higher than the IT wire cost.

At present the IT RRP® by OST and PIT by Bruker-EAS are the two processes of Nb_3Sn composite wires with sufficiently high J_c for HEP applications that are available in large quantities from industry.

B. Reaction Cycle

In all methods the Nb_3Sn phase is produced during a final multistage high-temperature heat treatment.

In any of today's state-of-the-art Nb_3Sn wire manufacturing, Nb_3Sn is formed by solid diffusion at high temperature (650°C or higher). In the binary Nb-Sn system single-phase Nb_3Sn layers form only above ~930°C, where the only stable phase is Nb_3Sn. At temperatures below 845°C, the two non-superconducting phases $NbSn_2$ and Nb_6Sn_5 are also stable and all three phases will grow at the interface, with $NbSn_2$ most rapidly formed and Nb_3Sn being the slowest. However, in the ternary system (Nb-Cu-Sn) the only relevant stable phase is Nb_3Sn even at lower temperatures. The diffusion path from the Cu-Sn solid solution to the Nb-Sn solid solution passes through only the A15 phase field, destabilizing the formation of the non-superconductive phases $NbSn_2$ and Nb_6Sn_5. Therefore, the addition of Cu lowers the A15 formation temperature from well above 930°C to any other that is deemed practical, thereby limiting grain growth and thus retaining a higher grain boundary density required for flux pinning. To the first order, the addition of Cu does not dramatically change the superconducting behavior of wires as compared to binary systems.

1) Heat Treatment Optimization

The reaction cycle required to produce the superconducting Nb_3Sn phase is a critical step in the manufacturing process of a magnet, i.e. the superconducting and mechanical properties of the superconductor are obtained during this operation, and it is a time consuming operation involving expensive tooling. The HT cycle for Nb_3Sn strands had been originally optimized at relatively low temperatures (<650°C) due to restrictions on the conductor insulation. Development of high temperature insulating materials has allowed increasing reaction temperatures up to 700°C, thereby reducing times, without a significant degradation of strand performance.

During HT, several Cu-Sn phases are created and eliminated in the course of Cu-Sn diffusion and Nb_3Sn formation processes. Attention has to be paid to prevention of thermally induced wire damage. For instance, the presence of liquid phases may cause motion of Nb filaments, allowing contact with adjacent ones, and the presence of voids may hinder the diffusion process. In addition, wire bursts due to liquid phases overpressure can damage the wires. These problems are solved by using multistage HT cycles.

In order to program the low temperature steps of the HT for Nb_3Sn composite wires, the growth kinetics of Cu-Sn phases was studied as a function of HT duration and temperature, and the diffusion constants of ε, η and δ phases were evaluated within their temperature ranges of solid diffusion [21]. The equation relating the thickness, y, of an intermetallic layer with time t, is:

$$y^2 = k_0(\exp(-E/\beta T))t,$$

where y is the intermetallic layer thickness, t is the duration and T is the temperature of the HT, k_0 is the diffusion frequency, β is the Boltzmann constant and E is the activation energy. Fig. 1 shows an example of η and ε formation at the Cu/Sn interface.

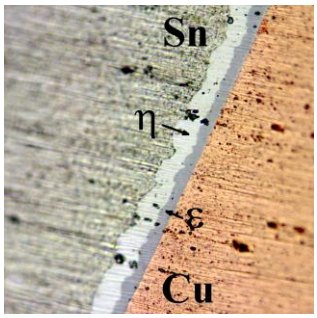

Fig. 1. Intermetallic growth at the Cu/Sn interface after 7 days at 210°C [21].

In addition to diffusing the Sn into the Cu, the low temperature steps of the HT should be optimized to also prevent leakage of Sn rich liquid phases, which is relevant for high J_c Nb_3Sn strands. A way to prevent leaks of Sn rich phases, which are characterized by low melting points, is to convert them into higher melting point phases. In wires, one week at 210°C, which is often suggested by manufacturers, leaves a large fraction of the Sn still unreacted. Instead, the Sn and the η phase can be converted into the higher melting point ε phase and some traces of α phase substantially faster at 400°C. At such temperature, less than a day is adequate for total conversion without the liquid phases reaching the filaments. However, crossing the Sn melting temperature during a direct ramp to 400°C is sufficient to create Sn leakages in cables. In order to prevent this, temperature dwells

below 227°C allow formation of an ε phase thin layer that works as a container against the overpressure of the liquid Sn above 227°C. Since the ε phase thickness formed at 210°C after 1 week is only about 1 μm larger than that formed after 3 days, a 3 day 210°C dwell followed by a 1 day at 400°C not only appropriately diffuses the Sn through the Cu, but also prevents Sn leaks, as experimentally confirmed on cables.

The investigation of the kinetics of phase growth also showed that for temperatures above 440°C, the δ phase growth is associated with the formation of voids and segregations that may result in cracks along the diffusion path. Since this phenomenon hinders the diffusion process between Cu and Sn, Cu-Sn diffusion in Nb_3Sn wires should be performed below 440°C.

2) Partial Wire Reaction

The study above motivated to explore feasibility of using partly reacted Nb_3Sn wires to reduce coil reaction and thus magnet manufacturing time. A MJR and an IT Nb_3Sn strands were partially reacted to convert the Sn to the η and ε phases, and then plastically deformed to estimate the amount of cabling and/or winding degradation. After completion of the reaction cycle at 700°C, the I_c was measured and compared with the I_c of samples reacted in an uninterrupted cycle. No I_c degradation was observed with preliminary heat treatments at 210°C for 1 week in a pure solid/solid diffusion process and at 400°C for 48 h in a liquid/solid diffusion process [22]. Fig. 2 shows cross sections of the IT strand at the end of the preliminary treatment. After 7 days at 210°C (left), a substantial part of the Sn is still unreacted. After 2 days at 400°C (right) the Sn has been completely converted into ε phase. Some voids formed during the reaction in the ε phase.

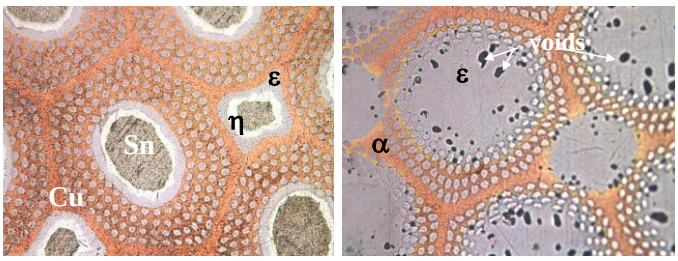

Fig. 2. Intermetallic growth in the IT strand after 7 days at 210°C (left), and after 2 days at 400°C (right). Some voids can be seen in the latter [22].

C. Main Parameters and Properties

The most important technical parameters which define the performance of a composite wire of diameter D include critical current density $J_c(B,T)$, magnetization $M(B,dB/dt)$, effective filament diameter d_{eff}, filament twist pitch l_p, superconductor fraction λ or Cu/non-Cu ratio, matrix axial ρ_n and transverse ρ_e resistivities, and Residual Resistivity Ratio RRR. Since Nb_3Sn require final heat treatment, the parameters of the heat treatment cycle are essential to achieve an optimal J_c and RRR. Finally, the conductor cost is important too.

The *critical current density* J_c is a key parameter, which controls the current carrying capability, stability, magnetization and AC losses of a superconducting wire, and thus the performance of superconducting magnets. It depends on the superconductor microstructure. The resistive transition of a composite superconductor is smooth, which leads to some uncertainty in the definition of J_c. Several criteria were formulated to define J_c based on resistive transition (or voltage-current characteristic) measurements. The most commonly used criteria for superconducting magnets define J_c at the axial resistivity of 10^{-14} Ω·m, or at a given electric field.

The following parameterization of the critical current density, $J_c(B,T,\varepsilon)$, as a function of magnetic field B, temperature T and strain ε, is often used for Nb_3Sn [23]:

$$J_c(B,T,\varepsilon)=\frac{C(\varepsilon)}{\sqrt{B}}\left[1-\frac{B}{B_{c2}(T,\varepsilon)}\right]^2\left[1-\left(\frac{T}{T_{c0}(\varepsilon)}\right)^2\right]^2,$$

where $C(\varepsilon)$ and $B_{c2}(T,\varepsilon)$ are expressed as follows:

$$C(\varepsilon)=C(I_{REF}(\varepsilon),B_{c20}(\varepsilon),T_{c0}(\varepsilon))=\frac{I_{REF}(\varepsilon)\sqrt{12T}}{\left[1-\frac{12T}{B_{c2}(4.2K,\varepsilon)}\right]^2\left[1-\left(\frac{4.2K}{T_{c0}(\varepsilon)}\right)^2\right]^2}$$

$$\frac{B_{c2}(T,\varepsilon)}{B_{c20}(\varepsilon)}=\left[1-\left(\frac{T}{T_{c0}(\varepsilon)}\right)^2\right]\left\{1-0.31\left(\frac{T}{T_{c0}(\varepsilon)}\right)^2\left[1-1.77\ln\left(\frac{T}{T_{c0}(\varepsilon)}\right)\right]\right\}$$

This empirical expression was obtained by Summers et al. in 1991 using Kramer, Ekin and Hampshire, and an empirical T dependence derived by Gorkov in 1959 from the microscopic theory. Other empirical scaling laws were proposed to parameterize the I_c data [24]. One of the practical purposes of parametrization is that of calculating the expected performance of a magnet from I_c measurements of strand samples used as witnesses during coil reaction. The intersection of the critical surface of each coil at the various magnet test temperatures with the B_{peak} load line of the magnet produces the expected coil short sample limit (SSL) at that temperature. SSL values typically have very little sensitivity to the scaling law that is used.

The *engineering current density* J_E is defined as the critical current density per total conductor cross section. It depends on the superconductor J_c and superconductor fraction λ or Cu/non-Cu ratio in the composite cross section.

Magnetization. A composite superconductor placed in a varying magnetic field becomes magnetized [19] with a magnetization described by the following formula:

$$M(B,\dot{B})=-\mu_0\left[\frac{2}{3\pi}\lambda J_c(B)d_{sc}+\frac{l_p^2\dot{B}}{4\pi^2\rho(B)}\right],$$

where d_{sc} is the filament diameter, l_p is the filament twist pitch, $\rho(B)$ is the effective transverse resistivity of the matrix, and $J_c(B)$ is the critical current density in the superconductor. The first term represents the component related to persistent currents in the superconducting filaments, and the second term represents the component associated with coupling eddy currents between filaments. Both components are diamagnetic in an increasing field and paramagnetic in a decreasing field. Composite wire magnetization plays an important role in superconducting accelerator magnets [25], which have demanding requirements on field uniformity. It is to be noted that in Nb_3Sn d_{sc} is indicated as d_{eff} (see below), since contrary to NbTi, the filament size is not always identical to its geometric size.

Magnetic hysteresis leads to energy dissipation in superconducting composites [21]. Similarly to magnetization, the power of AC losses P in a composite superconductor has two main components related to persistent and coupling eddy currents. The AC loss power per unit volume of composite wire after full flux penetration in superconducting filaments can be represented as follows:

$$P(B,\dot{B}) \cong \frac{2}{3\pi}\mu_0\lambda J_c(B) d_{sc}\dot{B} + \frac{\mu_0 l_p^2 \dot{B}^2}{4\pi^2\rho(B)}.$$

AC losses in composite superconductors play an important role in the thermal stabilization of superconducting coils during magnet operation and quench, and contribute to the heat load on a magnet cooling system.

The *effective filament diameter* d_{eff} impacts the level of wire magnetization and its effect on magnet field quality at low fields, as well as conductor stability against flux jumps. The d_{eff} can be obtained from the width of the magnetization loop $\Delta M(B) \propto J_c(B) \cdot d_{eff}$ using a measured $J_c(B)$ dependence. At present, the d_{eff} of Nb_3Sn strands with high J_c is still quite large (~50 to 100 μm to be compared with ~5 μm in NbTi wires) for both the IT and the PIT processes. The reduction of d_{eff} is limited in IT and PIT wires by the wire architecture and specifics of the manufacturing processes.

Analysis of stability of the superconducting state with respect to small field or temperature perturbations [19] has led to the following adiabatic stability criterion for the maximum transverse size d_{max} of a hard Type II superconductor:

$$d_{max} < \frac{\pi}{2}\sqrt{\frac{C_p(B,T)\cdot(T_c(B)-T_b)}{\mu_0 J_c(B)^2}},$$

where $C_p(B,T)$ is the superconductor specific heat, $J_c(B)$ and $T_c(B)$ are the superconductor critical parameters and T_b is the helium bath temperature.

The *wire diameter D* defines the critical current I_c that the wire can carry and thus the number of turns in a magnet. Flux jumps limit not only the size of the superconducting filaments but also the size of a multifilament composite wire due to self-field instability. The typical value of D for IT and PIT wires at present is 0.5 to 1.0 mm.

The self-field adiabatic stability criterion [19] sets the following upper limit D_{max} for the diameter of a composite wire:

$$D_{max} < \sqrt{\frac{32 C_p(B,T)\cdot(T_c(B)-T_b)}{\mu_0\lambda J_c(B)^2(-2\ln(1-i)-2i-i^2)}},$$

where λ is the fraction of superconductor in the composite cross section, $C_p(B,T)$ is the composite specific heat, and i is the ratio of transport current I_T to critical current I_c.

The *filament twist pitch* l_p controls the eddy currents in superconducting composites when subjected to varying magnetic fields, and hence the wire magnetization and AC losses. The typical value of twist pitch in superconducting composite wires is ~$10 \cdot D$, which is sufficient to suppress eddy current effects to an acceptable level.

The *Cu to non-Cu ratio* is an important parameter for strand stabilization and for magnet quench protection. It is also play an important role in processing of multifilament composite wires. A high Cu/non-Cu ratio is required to restrict the maximum temperature in the coil and the voltages in the magnet during quench. It also improves the strand stability with respect to the thermal perturbations in the coil. However, a low Cu/non-Cu ratio increases the fraction of superconductor in the coil and, thus, reduces the coil volume.

The *matrix axial resistivity* ρ_n determines the voltage and Joule heating power generated in a composite wire by the transport current during the superconductor transition from superconducting to normal state. The *transverse resistivity* ρ_e determines the level of eddy currents and thus eddy current magnetization and AC loss power in composite wires. These two parameters are related as follows [26]:

$$\rho_m \frac{1-\lambda}{1+\lambda} \le \rho_e \le \rho_m \frac{1+\lambda}{1-\lambda}$$

The *Residual Resistivity Ratio (RRR)*, defined as the ratio of the Cu matrix resistivity at room temperature R_{300} to its residual resistivity $R_{4.2}$ at T=4.2 K, is a measure of Cu matrix purity, which is important for strand stabilization and magnet quench protection. Typical values of *RRR* for PIT and IT are of about 200. The *RRR* depends on the amount of Sn in the billet, on the diffusion barrier thickness and on the heat treatment cycle. A low *RRR* indicates damage of the internal structure of the strand and Sn leakage into the surrounding Cu stabilizer. The RRR is also subject to magneto-resistivity, i.e. its value strongly decreases at increasing magnetic fields, and can be affected also by cabling.

The *reaction cycle* for Nb_3Sn strands includes the temperature profile, temperature ramp rate, uniformity and duration. Heat treatment studies and optimization for IT and PIT wire allowed substantial reduction of the reaction time without a substantial degradation of the strand performance. Reduction of reaction time is very important for magnet cost saving.

The *cost* of Nb_3Sn strands exceeds the cost of NbTi strands by a factor of 5 to 10. A significant reduction of Nb_3Sn wire cost is required to make this technology fully attractive for large superconducting accelerators. Taking into account that the fabrication technology of Nb_3Sn strands is similar to that of NbTi strands and that it does not use any rare or expensive components, it is believed that the present Nb_3Sn strand cost could be reduced by a factor of 2 to 3 from the present value. A sizable reduction of Nb_3Sn strand cost is also expected at large-scale production. A cost analysis of composite wires used in high-field magnets can be found in [27].

D. Nb_3Sn Wire R&D Programs

In 1999 the U.S. Department of Energy has started the Conductor Development Program (CDP) [28] as a collaborative effort of U.S. industry, national laboratories and universities with the goal of increasing the critical current density of Nb_3Sn IT wires. The target Nb_3Sn strand parameters for the superconductor R&D efforts by CDP are summarized below:

- Non-copper ,J_c at 12 T and 4.2 K – 3000 A/mm^2

- Effective filament size – < 40 microns
- Strand unit length – > 10 km
- Heat treatment time – < 200 h
- Conductor cost – < $1.50 kA-m (12 T, 4.2 K)

As a result of this program, multifilament IT Nb_3Sn wires produced using the Restack Rod Process (RRP®) by OST, demonstrated critical current density J_c above 3 kA/mm^2 at 12 T and 4.2 K [9], [29]. In parallel the CDP was focused on the optimization of J_c, Cu matrix *RRR*, effective filament diameter d_{eff} and subelement spacing to develop strands for 10 to 12 T superconducting magnets stable with respect to flux jumps.

At the same time DOE funded Nb_3Sn strand design and technology development in the framework of the Small Business Innovation Research (SBIR) program [30]. The SBIR was focused on the IT and PIT wires, improving wire J_c, increasing stability and lowering wire magnetization and AC losses by reducing the d_{eff} (increase the number of subelements), etc.

A parallel effort started in early 2000s in the European Union as part of the Next European Dipole (NED) program [18]. This effort was focused on the development of composite Nb_3Sn wires of large diameter (wire diameter up to 1.25 mm) with a J_c of 1.5 kA/mm^2 at the higher field of 15 T and 4.2 K produced by two methods: Enhanced Internal Tin (EIT) [31] and Powder in Tube (PIT) [32]. The target Nb_3Sn strand parameters for the NED superconductor R&D efforts are summarized below:

- Non-copper J_c at 15 T and 4.2 K – 1500 A/mm^2
- Effective filament size – < 50 microns
- Wire diameter – 1.250 mm
- RRR – >200
- Strand unit length – > 50 kg

At present this effort, led by CERN, is concentrating on optimization of PIT wires at Bruker-EAS.

The Nb_3Sn conductor development was also carried out on a smaller level in Japan, focusing on the combination of J_c at 12 T and 4.2 K, high *RRR* and small d_{eff} using the Distributed Tin (DT) method [33].

E. Commercial Nb_3Sn Wires

1) Internal Tin RRP® Wires

IT wires were produced by several companies. In the US it was done mainly by IGC and OST. Optimization of the IT strand design and of its processing, fostered by the US DOE Conductor Development Program (CDP), produced a fast progress in J_c at 12 T and 4.2 K from ~1500 A/mm^2 to more than 3000 A/mm^2 from 1999 to 2006 (see Fig. 3).

The development of IT wires, mostly focusing on IT wires from Oxford Instruments Superconducting Technology (OST), was reviewed elsewhere [34]. OST has been producing IT Nb_3Sn using two basic approaches: single diffusion barrier and distributed diffusion barrier. The former is ideal to produce the low hysteresis losses required for ITER magnets, and the latter is used in applications where J_c is the most important property.

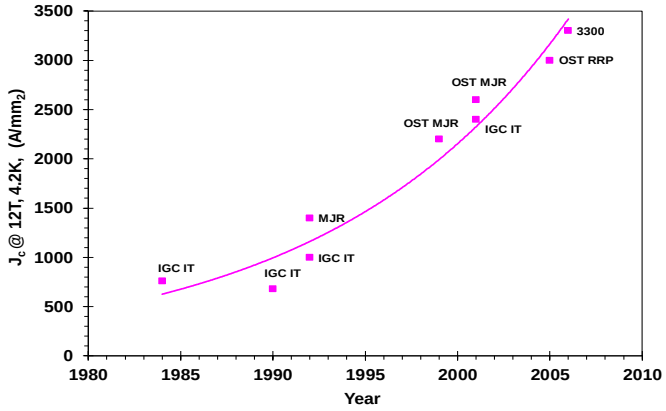

Fig. 3. J_c as a function of time for IT Nb_3Sn. The highest J_c of 3300 A/mm^2 was first obtained by OST in a 0.7 mm wire of RRP® design with 61 restacks.

For particle accelerator magnets, over the past ten years OST has produced several tons of 54/61 configuration high J_c RRP® strand for HEP applications. RRP® is a distributed barrier IT strand having a Nb based diffusion barrier, therefore the subelement size d_{SE} is a good approximation for the d_{eff}. At 0.8 mm size this wire had a d_{SE} ~ 80μm. When the impact of d_{eff} on magnet stability at low field became fully apparent in the accelerator magnet community, OST focused on increasing billet stack count while maintaining at the same time volume scalable processes. To reduce subelement merging during cabling, the Cu spacing between subelements was also increased. Fig. 4 shows a conceptual schematic of this R&D work. A second generation strand with 127 stack design entered production in 2008, with several tons utilized in HEP at 0.7 to 0.8 mm diameter and d_{SE} of 45 to 52 μm. A third generation wire with 169 stack design followed in 2011 [35]. This wire has d_{SE} of 40 to 58 μm for sizes of 0.7 to 1 mm. Integrated volume production of 169 stack RRP® billets at OST is approaching that of the 127 stack billets. Cross sections of wire designs produced by OST are shown in Fig. 5.

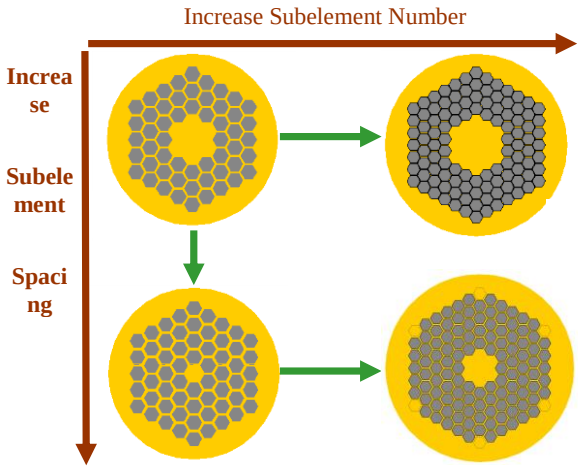

Fig. 4. Schematic of R&D performed by OST in collaboration with FNAL on RRP® wires to reduce their d_{eff}.

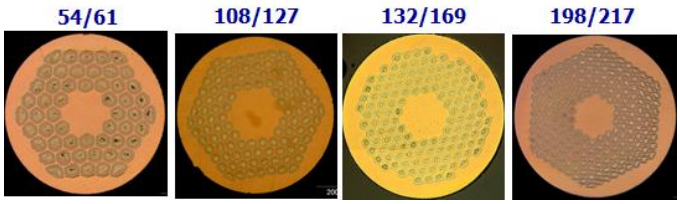

Fig. 5. Cross sections of RRP® wires designed at OST (courtesy of OST).

OST has switched from using NbTa alloy for the Nb filaments to Ti-doped strand, which is optimized at lower reaction temperatures (~665°C) with respect to Ta-doped wire (~695°C) [35]. Another reason is the improved irreversible strain limit for the former.

To preserve *RRR*, OST has also been working on optimizing the Sn fraction in the billet, as well as the barrier thickness [35]. Unfortunately, with the present subelement design, holding *RRR*>100 as d_{SE} decreases results in lower J_c, as evidenced in the plot of Fig. 6. This is caused by the need to under-react to preserve *RRR*, the need for higher Nb:Sn ratios, and smaller Sn diffusion channels.

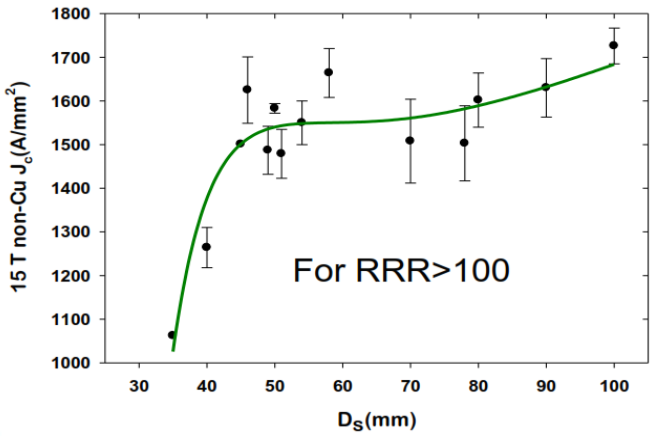

Fig. 6. Average RRP® J_c(4.2K, 15 T) as function of subelement size when imposing *RRR*>100 [35].

2) Powder-in-Tube Wires

The history and development of PIT wires was reviewed elsewhere [11]. The PIT process was first developed by the Netherlands Energy Research Foundation (ECN) and further optimized by the Shape Metal Innovation Company (SMI). Bruker-European Advanced Superconductors (Bruker-EAS) in Germany recently purchased the Technology Transfer with the goal of mass-production. The J_c as a function of time for binary and ternary $NbSn_2$ powder based PIT processed wires is shown in Fig. 7. The development of this technique has allowed producing in the laboratory long 192 filament strands. Shorter samples of 1332 filament strands were also obtained [14]. This method could allow an optimal combination of small filament size (<50 μm) and high J_c comparable to the IT process. Wires can presently be manufactured at SMI/EAS in about 45 kg net production units. The maximum non-Cu J_c has recently surpassed 2600 A/mm^2 in 1.25 mm wires with 288 filaments of 35 μm, developed for the Next European Dipole (NED) program. PIT wires produced by SMI and now by Bruker-EAS are shown in Fig. 8. The last two in Figure are being considered for use in Nb_3Sn 11 T dipoles and 150-mm aperture quadrupoles developed for LHC upgrades.

PIT wires were also produced in the U.S. at Supercon Shrewsbury (MA), SupraMagnetics (CT) and Supergenics (MA). The R&D work on these wire was partially funded by the SBIR program.

Supercon replaced $NbSn_2$ powder with alternative powders, renaming the process as Internal-Tin-Tube process. Non-Cu J_c values of 1800 A/mm^2 at 12 T and 4.2 K were achieved in this layout.

SupraMagnetics has been making PIT wires with jet milled Cu_5Sn_4 powder, which provides more Sn for the reaction compared to the $NbSn_2$ powder. Monel and Glid Cop Al-15 are options used to internally strengthen the wires. Non-Cu J_c values close to 2500 A/mm^2 at 12 T and 4.2 K were achieved.

Supergenics, in collaboration with HyperTech Research (OH), was developing PIT-like wires by employing pure Sn and Sn-alloy cores as a Sn source. Wires with 246+25 filaments at 18 μm carried a maximum non-Cu J_c at 12 T and 4.2 K of 2050 A/mm^2, whereas versions with 35 μm filaments achieved 2250 A/mm^2.

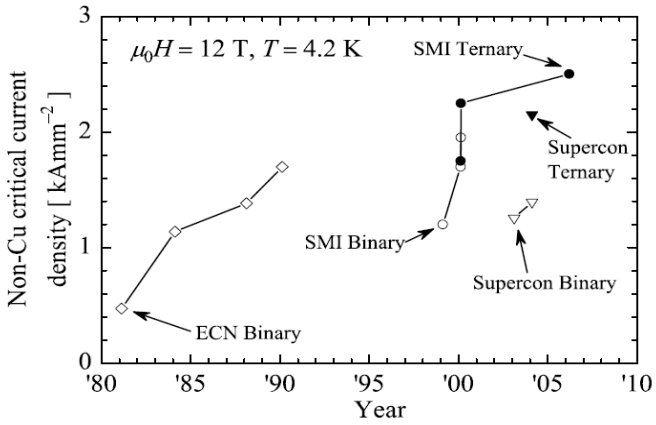

Fig. 7. Non-Cu J_c as a function of time for binary and ternary $NbSn_2$ powder based PIT processed wires [11].

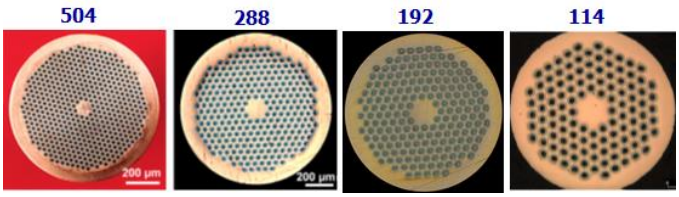

Fig. 8. Cross sections of PIT wires of different designs (courtesy of SMI and Bruker-EAS).

III. Nb_3Sn Wire Properties

In this section, we detail those key research activities and methods used in the International community that helped study and solve most of the aspects required of Nb_3Sn wires for magnet realization. This includes I_c and J_c improvements, *RRR* effects, strain sensitivity, magnetization and stability to flux jumps.

A. I_c, J_c Improvement

Whereas both T_{co} and B_{c20} depend on the material chemical composition, J_c rests also on the superconductor microstructure, which controls the flux pinning mechanisms. In particular, in 1975 it was shown by Scanlan et al. [36] that J_c in bronze processed Nb_3Sn is inversely proportional to grain size. In 1976 Pande and Suenaga [37] predicted that after going through a maximum the J_c decreases for smaller grain sizes. Later experiments [38, 39] confirmed that the J_c decreased for grain sizes below ~50 nm.

1) Flux Pinning Models

NbTi and Nb_3Sn feature very different scaling behavior with respect to magnetic flux density and temperature [19, 23, 40-44]. Experimental studies [40, 42, 45-46] have found that A15 materials, such as Nb_3Sn, consist mainly of radial and equiaxed superconducting grains separated by layers ~2 nm thick. As stressed by Dew-Hughes [40], the elongated, axial structure of cell walls found in NbTi seems to lead exclusively to 'transverse pinning', while the equiaxed grain structure of Nb_3Sn tends to lead to 'longitudinal pinning' behavior over most of the field regime. Many authors have attributed this difference to different mechanisms for flux motion [40-41, 43]: the scaling behavior of NbTi has been associated with pin breaking, while that of Nb_3Sn has been identified with flux shearing. For instance, Kramer's model (1972) is based on flux shear. If the pin-breaking force exceeds the shear strength of the lattice, flux flow will occur by shear. However, it was known that this model used questionable assumptions (for instance a high field limit for the shear modulus), required unrealistic physics parameters, most notably it did not contain the observed grain-size dependence of J_c, and employed an expression for the shear modulus valid only at high fields. These various deficiencies have left the physical picture somewhat incomplete [40] and since then, a number of additional attempts were made to explain the observed $J_c(B, T)$ by either flux shearing or pin breaking (Dew-Hughes, Suenaga, Evetts and Plummer).

Many of the observed features of the magnetic and transport properties of Nb_3Sn, as well as of other A15 materials, could be understood by modeling them as a collection of strongly coupled superconducting grains and taking into account the anisotropic flux pinning by grain boundaries [47]. Because of the strong coupling of the grains, the junctions were treated within the framework of nonlocal Josephson electrodynamics (NLJE). Each junction was described by a maximum Josephson current density J_0, above which the gauge-invariant phase difference across the junction, $\Delta\gamma$, starts to slip leading to a voltage drop. In this model, J_c is determined solely by grain boundary pinning. Nevertheless, this single mechanism leads to two different scaling laws because of the anisotropy of the pinning forces. This approach led to the observed scaling behavior of Nb_3Sn over a majority of the field range, provided a clear physical picture of its origin by reproducing many of the features seen experimentally, as well as a plausible explanation for the deviations at low and high fields and at high temperatures.

2) IT Composite Wires

The J_c of IT Nb_3Sn is affected by design parameters such as subelement size, number of restacks, relative amount of Sn and Nb in the non-Cu section, and type of ternary material in the Nb_3Sn. To reach high J_c values, both the quantity (the amount of superconductor that is formed in the non-Cu fraction) and the quality (grain refinement, Sn content, and ternary element addition) of the Nb_3Sn must be optimized. This is possible by reducing the fraction of Cu in the matrix to a practical manufacturing minimum in the range of 0.1 to 0.3, by introducing alloying additions such as Ta or Ti, and by an optimized HT schedule. Furthermore, the barrier that separates the multifilamentary regions from the high-purity Cu is made of Nb and is partially reacted during heat treatment, thus adding to the final superconducting cross section. After HT, the tightly packed Nb filaments and the reacted portion of the barrier grow into a completely connected volume of Nb_3Sn, fully coupled, and whose typical dimension is approximately the size of the stacked subelement.

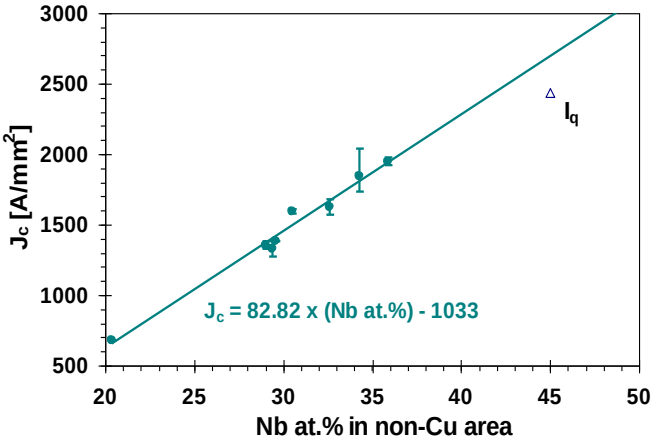

Fig. 9. J_c (12 T, 4.2K) values plotted against Nb content in the wire as produced by different IT strands having undergone similar HT cycles.

The J_c of IT strands is proportional to the atomic percentage of Nb in the non-Cu area of a wire. This is clearly shown in Fig. 9, where the J_c (12 T, 4.2K) values plotted against Nb content in the wire were produced by different IT strands having undergone similar HT cycles. To reach a J_c of 3000 A/mm^2 requires about 50 at.% Nb with the present IT technology. Also, the maximum achievable intrinsic J_c (12 T, 4.2K) can be estimated at around 5000 A/mm^2 by extrapolation to 75 at.% Nb in the non-Cu area (*i.e.* physical limit on Nb content imposed by stoichiometry).

A larger number of subelements in the strand appeared to increase heat treatment efficiency in forming the Nb_3Sn A15 phase. This was inferred by the different times needed by 19 subelement designs with respect to 37 or 61 subelement designs to reach the peak J_c. Whereas the former required 50 to 70 h, the latter needed only 40 to 50 h.

3) PIT Composite Wires

The J_c of PIT Nb_3Sn is affected by design parameters such as filament size, number of Nb tubes, use of binary or ternary $(NbTa)_3Sn$ and quality and size of the $NbSn_2$ powder.

An interesting experiment showed for instance how to optimize filament size for J_c in PIT wires [48]. This can be

done by measuring the superconducting layer thickness and associated layer J_c as function of reaction time and temperature. Since at a given reaction temperature the layer J_c appears to peak with time and then decrease, the corresponding size of the superconducting layer formed at the temperature that produced the maximum J_c is a good indication of filament thickness required in the wire design. Fig. 01 shows this method for 1 mm PIT wires with 192 tubes of ~50 μm outer diameter and thickness of 12 to 13 μm. The layer J_c peaked at a reaction temperature of 700°C, at which a superconducting layer formed of ~ 10 to 11 μm. This wire was well-designed as it allowed for 2 to 3 μm of outer unreacted Nb in the tubes in order to preserve *RRR*.

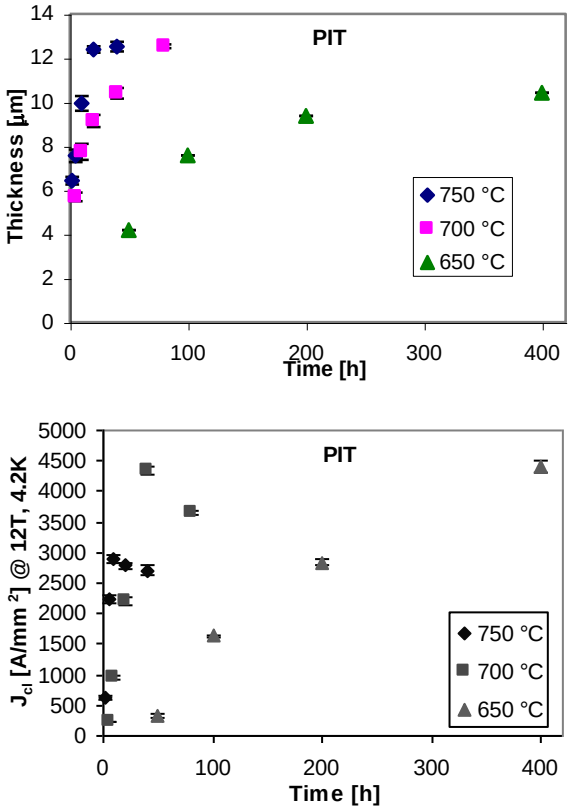

Fig. 10. Nb_3Sn layer growth (top) and layer J_c at 12 T and 4.2 K (bottom) as a function of HT time and temperature for a 1 mm PIT wire with ~50 μm Nb tubes [48].

B. *RRR*

The *RRR* is a means to measure strand Cu purity, which is important for strand stabilization and magnet quench protection. Typical values for the present technologies are of about 200 for PIT and IT. For IT, the *RRR* depends strongly on the amount of Sn in the billet and on Nb barrier thickness, ranging from about 20, to 60, to 160 for barrier thicknesses of 3, 4.2 and 6 μm respectively. A low *RRR* indicates damage of the internal structure of the strand and Sn leakage into the surrounding Cu stabilizer. The *RRR* of round wires was found to depend on the heat treatment cycle [49]. However, the *RRR* reduces after cabling, and especially locally at the edges of the cable, and is also subject to magneto-resistivity (see Fig. 11), i.e. its value strongly decreases at increasing magnetic fields.

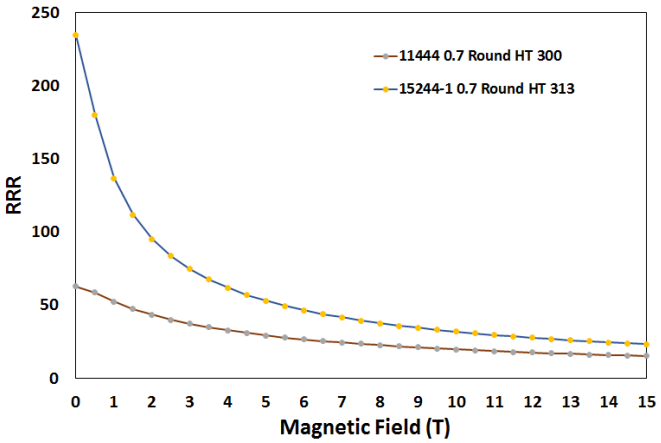

Fig. 11. *RRR* vs. *B* measured using 0.7 mm RRP® wires at FNAL (courtesy of D. Turrioni).

C. *Stress/strain Sensitivity*

The A15 cubic crystal structure is modified by strain into a tetragonal phase, which causes a reduction of the intrinsic superconducting properties of the compound. The produced distortions, whose energy is on the scale of the mRydberg, move the Fermi energy E_F to higher values with respect to the undeformed cubic phase. It is known that such variations are correlated to strain-induced modifications in both the phononic and electronic properties. The strain-induced modifications in the average phonon frequencies and in the bare electronic density of states $N(E_F)$ at the Fermi energy contribute to strain-induced degradation of T_c in Nb_3Sn [50]. It was recently shown from data analysis of Nb_3Sn samples that $N(E_F)$ decreased by 15 to 30% as T_c varied from 17.4 to 16.6 K under external axial strain, and that the relationship between $N(E_F)$ and T_c in strained Nb_3Sn strands shows significant difference between tensile and compressive loads [51]. Because higher magnetic fields produce proportionally higher Lorentz forces, 3D strain sensitivity of critical current is a very important property in superconductors. In addition, Nb_3Sn is brittle. In bulk form it fractures at a tensile strain of ~ 0.3%. In filamentary form, when supported by a surrounding matrix, it can be strained to ~ 0.7% before fracture.

1) *Tensile/compressive Strain Degradation*

The strain behavior for a number of Nb_3Sn RRP® wires is shown in Fig. 12 [52], which presents the normalized I_c(4.2K,15T) vs. axial intrinsic strain. The irreversible strain can be also identified. The irreversible intrinsic strain of Ta-doped Nb_3Sn wires is less than +0.11%, to be compared with the irreversible intrinsic strain range of +0.26% to +0.31% found for Ti-doped wires, consistently with NIST studies [53].

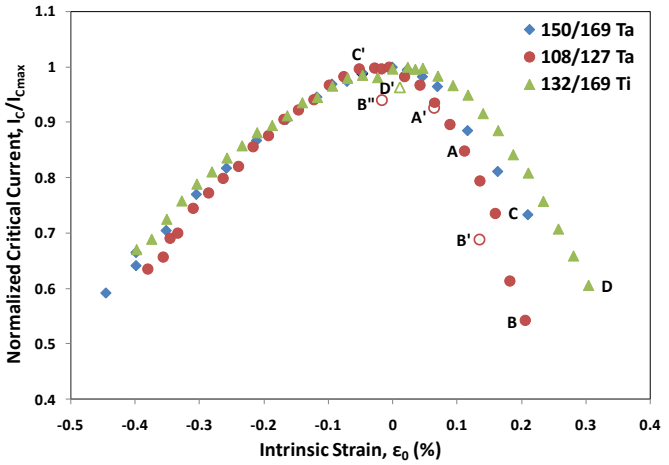

Fig. 12. Normalized I_c(4.2 K, 15 T) as a function of longitudinal intrinsic strain for 0.7 mm samples of Ta-alloyed 108/127 RRP®, Ta-alloyed 150/169 RRP® and Ti-doped 132/169 RRP® wires [52].

2) Bending Degradation

The I_c degradation of Nb_3Sn due to bending is important when using Nb_3Sn with the React&Wind technique as opposed to the Wind&React approach. In the former a magnet is wound with an unreacted cable, in the latter the cable is reacted on a spool of given diameter before being used for winding the coils. Bending degradation was measured in [54], by reacting Nb_3Sn wire samples on smaller sample holders than those used for I_c measurements. The results of I_c measurements made on unbent strands were compared with those made on IT and MJR wires with a maximum bending strain of about 0.2% and 0.4%. Based on these data, for React&Wind magnets that featured a minimum bending radius of 90 mm (*i.e.* maximum bending strain of about 0.2% for a 0.7 mm wire), the bending degradation at 12T was expected to be less than 7% for the MJR material and less than 5% for the IT material [55].

Bending degradation was also measured on cables made of the same IT wire as above. The cables were reacted while bent on a 290 mm diameter reaction spool, and straightened before impregnation and measurement. Results were compared with those of unbent samples. An excellent correlation between strand and cable tests was found for cables without a resistive core, whose strand layers bent independently [56].

D. Wire Magnetization

As discussed above, practically all modern Nb_3Sn strands, due to technological constraints, have large effective filament diameter d_{eff}, which is responsible for the magnetization. Magnetization loops between 0 and 3 T for IT (MJR and RRP®) and PIT strands are shown in Fig. 13 per non-Cu volume. Flux jumps are seen for all the strands at low fields. These flux jumps lead to some field uncertainties at low field from cycle to cycle.

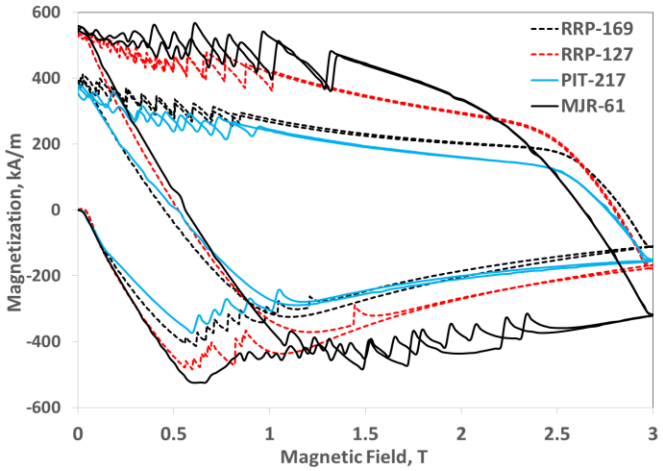

Fig. 13. Magnetization curves per non-Cu volume: a) MJR - 1 mm, d_{eff}~100 μm, J_c(12T,4.2K)~2000A/mm^2; b) PIT - 1 mm, d_{eff}~50 μm, J_c(12T,4.2K)~2100A/mm^2; c) RRP108/127 – 0.7 mm, d_{eff}~45 μm, J_c(12T,4.2K)~2900A/mm^2; and d) RRP150/169 – 0.7 mm, d_{eff}~40 μm, J_c(12T,4.2K)~2700A/mm^2.

The eddy current component of strand magnetization in Nb_3Sn composite wires is suppressed by using a small wire twist pitch. For l_p<15 mm and a rather low ρ_e~10^{-10} Ω·m, the eddy current magnetization component is less that 1% of the hysteretic component at dB/dt<0.1 T/s.

E. Flux Jump Stability

Flux jump instabilities impose limits on the superconductor transverse size. The maximum effective filament size for Nb_3Sn strands, calculated using adiabatic and dynamic stability criteria [19, 57], as a function of magnetic field are plotted in Fig. 14. According to both criteria, the filament size has to be 10 to 20 μm or less for J_c(12T,4.2K)>2 kA/mm^2 to avoid flux jumps in a Nb_3Sn strand at all fields. Thus, for all practical Nb_3Sn strands with d_{eff}~50 to 70 μm presently used in accelerator magnets, both criteria predict instabilities in a large field range: B < 6 to 8 T.

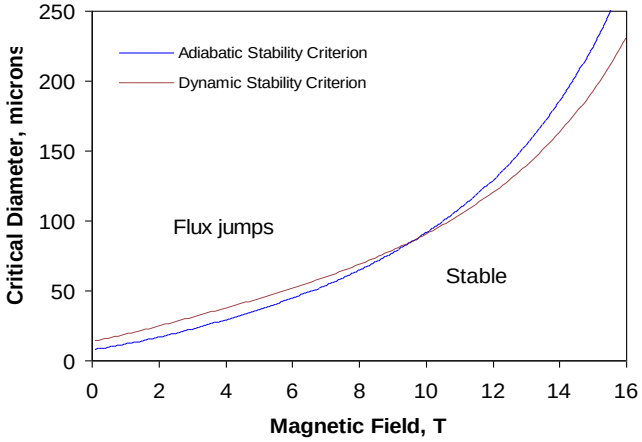

Fig. 14. Calculation of the maximum d_{eff} for a Nb_3Sn strand with J_c(12T,4.2K)=2 kA/mm^2.

Nevertheless, under certain conditions, a superconductor can carry some limited transport current in the presence of

partial flux jumps [58]. This was first shown theoretically by R. Hancox [59] in the 1960s using the enthalpy stabilization approach and the partial flux jump concept. Theoretical and semi-empirical studies of electromagnetic instabilities in modern Nb_3Sn strands are reported elsewhere [60-62]. An example of calculations of strand maximum transport current density $J_{ct}(B)$ in an external magnetic field for Nb_3Sn wires and magnet field limits is shown in Fig. 15 [63]. This model predicts significant reduction of strand current carrying capability at low fields with respect to its critical current density $J_c(B)$ for all Nb_3Sn strands used in recent accelerator magnet models. Furthermore, for strands with large d_{eff} and high J_c, the maximum transport current at low fields is smaller than the transport current at high fields.

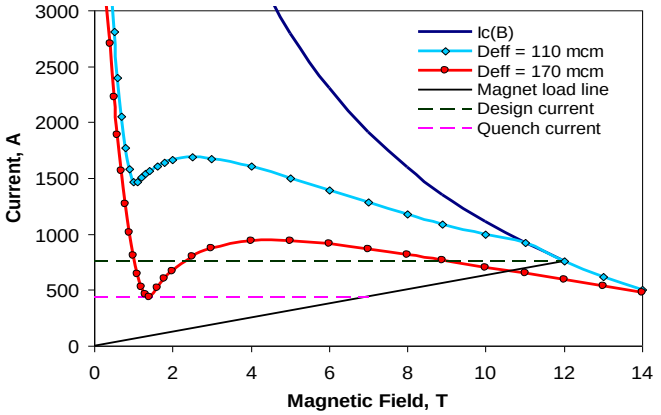

Fig. 15. Calculated maximum current in Nb_3Sn wires vs. field and maximum field for a magnet with flux jumps in conductor [63].

Unstable magnet performance occurs when the load line of a magnet encompasses an instability region in the *I* vs. *B* conductor behavior. Wires are indicatively used to determine the maximum quench current in the presence of a magnetic field variation by performing *V-H* tests in addition to standard *V-I* tests. In *V-H* tests the transport current is ramped to a fixed value, and the field is swept up and down between 0 and 4 T, typically with ramp rates of 5 to 17 mT/s. If no quench is observed the current is increased and the test repeated. I_S is defined as the minimum current at which a quench occurs during the above process.

The behavior presented in Fig. 15 was observed in Nb_3Sn wire measurements [58], [64]. A reasonably good correlation between the experimental data and the model predictions was found for Nb_3Sn wires with different J_c and d_{eff} produced using PIT, MJR, and RRP®.

The summary of a stability analysis [52] that used a majority of test results available to date on strands, cables and magnets, is shown in Table I. Values of subelement sizes of RRP® wires that produced stable Nb_3Sn magnet performance down to 1.9 K are indicated in bold, and in italic those that did not lead to optimal performance. The subelements values in between are shown in the framed boxes. In Table, d_{SE} represents the geometrical subelement size of the unreacted flat to flat dimension of the hexagonal outer diffusion barrier, as calculated at OST from design. From Table I the acceptable d_{SE} for Nb_3Sn accelerator magnets operating at 1.9 K to 4.5 K with a design field of 10 T or higher and high conductor critical current density J_c(12T, 4.2K) of 2500 A/mm^2 to 3000 A/mm^2 is 40 to 45 µm or less. Such d_{SE} range includes the combined effects of cable packing factor, J_c and *RRR* variations of cables used in magnet models.

TABLE I
SUBELEMENT SIZES IN RRP® MULTI-STACK STRANDS [52]

Stack design	Strand Sub-element size d_{SE}, µm				
	0.5 mm	0.6 mm	0.7 mm	0.8 mm	1.0 mm
61	**42**	51	59$^{\wedge *+}$	*68*$^{\wedge}$	*85*$^{\wedge *+}$
91	**34**	**41**	48$^{\wedge *}$	55$^{\wedge}$	*69*$^{\wedge}$
127	**29**	**35**	**41**$^{\wedge *+}$	47$^{\wedge}$	59$^{\wedge *+}$
169	**26**	**31**	**36**$^{\wedge *+}$	**42**$^{\wedge}$	52$^{\wedge}$
217	**23**	**27**	**32**	**36**	**45**

$^{\wedge}$ tested strand samples; * tested in cables; $^{+}$ tested in magnets.

In addition to producing stable magnet performance down to 1.9 K, wires with subelement values of ~40 µm or less produce coil re-magnetization at currents close to typical LHC injection currents, making for simpler corrections. Magnetic measurements of the Transfer Function and field harmonics of 11 T dipole models show that subelement values of ~40 µm are acceptable also for coil magnetization.

It was found experimentally that given the same J_c and d_{eff}, flux jumps depend also on the wire *RRR* [50]. The effect of the matrix *RRR* on J_c degradation due to flux jumps at low fields is shown in Fig. 16.

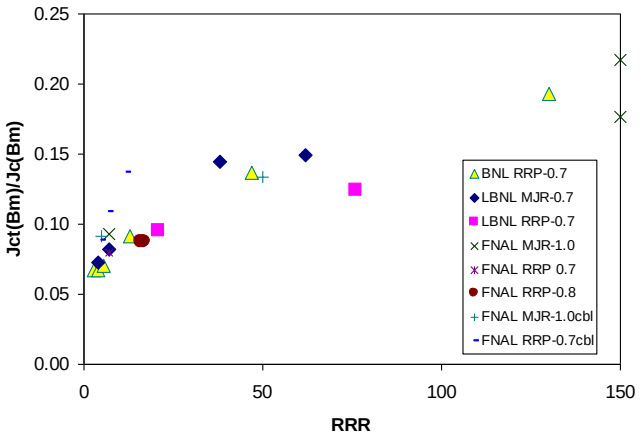

Fig. 16. Effect of matrix *RRR* on J_c degradation due to flux jumps at low fields.

A parametric study was performed by using Finite Element Modeling on strands having *RRR* between 30 and 265 [65] to quantify the effect of *RRR* on stability. The quench current at 4.3 K was computed for the minimum in the low field region and for 12 T in the case of self-field instability and large perturbations. According to this study, for *RRR* larger than 100, the instability at low field is not a problem for a magnet designed to work at 12 T (or larger fields). On the other hand, high field instability does not improve much by increasing the

RRR above 100 (partially due to the magneto-resistance effect dominating the electrical and thermal conductivity properties of the copper at high magnetic fields).

IV. Nb_3Sn Rutherford Cables

Three-side views and cross-sections of a 40-strand Nb_3Sn cable with keystoned cross section developed and fabricated at FNAL are shown in Fig. 17 [66].

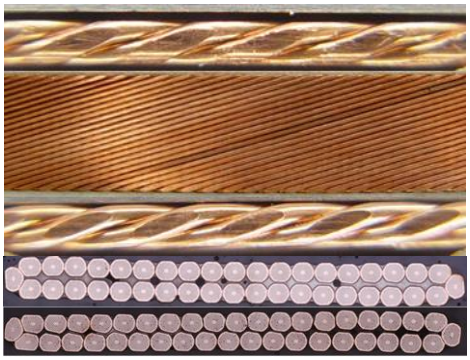

Fig. 17. Three-side views of a Nb_3Sn Rutherford cable with a keystoned cross section (top), cable rectangular (middle) and keystoned (bottom) cross sections [66].

In this section, we identify fundamental electromagnetic and geometric parameters of Nb_3Sn cables, including the effects from cabling on the strands and their subelements, briefly touch on quality control and summarize findings on cable change during heat treatment.

A. *Electromagnetic Parameters*

The maximum value of a cable critical current I_c is the sum of the strands critical currents I_{ci}. The actual total current I_c is somewhat lower, due to the degradation of strand performance during cabling g_i:

$$I_c = \sum_{i=0}^{N} g_i I_{ci} ,$$

where N is the number of strands in a cable.

Due to electromagnetic coupling between strands, the Rutherford cable magnetization and AC losses components include additional eddy current contributions controlled by the cable geometry and interstrand contact resistance [67]-[69]. The additional cable magnetization and loss power, caused by the inter-strand eddy currents in the cable, are determined by the following formulas:

$$\vec{M}_c = -\mu_0 \cdot \left(\frac{8}{15}\frac{\alpha^2 L^2}{\rho_c}\frac{d\vec{B}_\perp}{dt} + \frac{1}{3}\frac{L^2}{\rho_a}\frac{d\vec{B}_\perp}{dt} + \frac{1}{4}\frac{L^2}{\alpha^2\rho_a}\frac{d\vec{B}_{||}}{dt}\right),$$

$$P_c = \frac{8}{15}\frac{\alpha^2 L^2 \dot{B}_\perp^2}{\rho_c} + \frac{1}{3}\frac{L^2 \dot{B}_\perp^2}{\rho_a} + \frac{1}{4}\frac{L^2 \dot{B}_{||}^2}{\alpha^2\rho_a},$$

where $4L$ is the cable transposition pitch, α is the cable aspect ratio (the ratio of the cable width w to its mean thickness t), $B_\perp$ and $B_{||}$ are the perpendicular and parallel components of the magnetic field to the cable wide surface, and ρ_c and ρ_a are the effective cable resistivity between cable layers and within a layer respectively. The first term in both formulas provides the main contribution owing to the large value of α. The parameter ρ_c and the measurable value R_c [70] are related as follows:

$$\rho_c = \frac{4\alpha L}{N^2} R_c.$$

To control eddy current magnetization and losses in a Rutherford cable, it is necessary to increase the contact resistance. This can be done in Nb_3Sn cables by coating strands with metal, e.g. Cr, which survives a high-temperature heat treatment. However, good current sharing between strands requires low contact resistances. The optimal way of reducing eddy current effects in a Rutherford cable without worsening current sharing is to increase R_c while keeping R_a low. This is done by using a thin resistive core inside the cable [68], typically of stainless steel.

The most important parameters, which define the performance of a Rutherford cable in a magnet, include critical current I_c and average critical current density J_A, Cu/non-Cu ratio, cable axial normal resistivity ρ_n and Residual Resistivity Ratio *RRR*, and interstrand resistances R_c and R_a. As in the case of single Nb_3Sn composite wires, the parameters of the HT cycle, which affect I_c, *RRR* and contact resistances R_c and R_a, as well as cable cost, are also very important.

B. *Cable Design Parameters*

The Rutherford cable geometry is characterized by a cable aspect ratio α and a cross section area S_{cbl}, determined by its width w, mid thickness t and keystone angle φ, cable pitch angle θ, and cable packing factor *PF*.

Pitch or transposition angle θ. The cable pitch angle affects the cable mechanical stability and the critical current degradation. Typical values of pitch angle in NbTi cables used in accelerator magnets were within 13 to 17 degree. A special study of the possible pitch angle range for Rutherford cables was performed using 1 mm hard Cu strand and 28-strand cable design, and 27 and 39 strand cables with 0.7 mm Cu Alloy68 strand [71]. It was found that for 1 mm strands, below 12 degree the cable shows mechanical instability and that at 16 degree and over, popped strands, sharp edges and crossovers start occurring. In the case of 0.7 mm strands, the stable range of transposition angles was within 9 to 16 degrees.

Cable packing factor PF. The cable packing factor, *PF*, is defined as the ratio of the total cross section of the strands to the cable cross section envelope $S_{cbl} = w \cdot t$:

$$PF \cong \frac{\pi N \cdot D^2}{4(w \cdot t - A_{core}) \cdot \cos\theta},$$

where N is the number of strands in the cable, D is the strand diameter, w and t are the average cable width and thickness, θ is the cable transposition angle, and A_{core} the cross section area of the core.

The minimal *PF* for a Rutherford cable, i.e. one having a non-deformed cross section, has a value of $\sim\pi/4=0.785$. To provide cable mechanical stability and precise width and

thickness (parameters that are important for accelerator magnet coils), Rutherford cables are usually compacted by squeezing their cross section in both transverse directions. For an I_c degradation limited to 5 to 10%, increasing the cable *PF* allows raising also the cable average current density J_A, which is defined as follows:

$$J_A = I_c/S_{cbl}\,.$$

Cable edge and width deformation R_e, R_W. The critical current degradation is determined mainly by the amount of cable cross section deformation. The deformations of cable edge R_t and width R_w are defined as follows:

$$R_e = \frac{t}{2D}, \qquad R_w \cong \frac{2w\cdot cos\theta}{N\cdot D},$$

where D is the strand diameter, N is the number of strands in the cable (N=N+1 in the case of odd N), and θ is the cable transposition angle.

NbTi cables, which were used in the Tevatron, HERA, RHIC, UNK, SSC, and LHC, had a relatively large small edge deformation R_e~0.76 to 0.82. It was also experimentally established that the deformation of the cable width should be kept small, R_w~0.97 to 1.0. The *PF* of NbTi cables was quite high, typically within 88 to 93%. NbTi cables with cross section deformation in the above ranges have an I_c degradation of less than 5%. An additional important limitation on cable *PF* is related to cable sharp edges observed in cables with high *PF*s.

Large strand plastic deformations, which were acceptable for a ductile superconductor like NbTi, are not suitable for the more delicate Nb_3Sn strand structure. An example of strand cross section, as deformed after cabling, is shown in Fig. 18 (left) [63]. Fig. 18 (right) shows the local subelement deformations due to barrier breakage and merging observed in some RRP® Nb_3Sn strands.

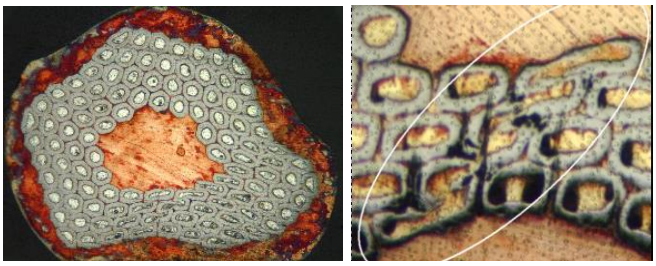

Fig. 18. Examples of deformed strand in a cable (left), and local subelement damage and merging (right) [63].

It has been found that the small edge deformation R_e in Nb_3Sn cables should be 0.85 or higher, and that the width deformation R_w should be slightly larger than 1.0, typically R_w=1.0 to 1.03, to avoid excessive strand deformation at the cable thin edge. The limits on small edge deformation and cable width define a value for the optimal keystone angle of the cable cross section. The nominal cable *PF* for Nb_3Sn cables is within 84 to 87%. This parameter space allows keeping the critical current degradation of Nb_3Sn Rutherford cables below 5 to 10%, and provides sufficient cable compaction to achieve adequate mechanical stability for coil winding, as well as high average critical density J_A.

Strand plastic deformation. By defining strand deformation ε_{str} as follows:

$$\varepsilon_{str} = \frac{d_{max}-d_{min}}{d_0},$$

where d_{max} and d_{min} are the longest and shortest diameters measured through the strand center, and d_0 is the original round strand size, a correlation could be found between the average deformation of all strands in a cable and its packing factor. This can be seen in Fig. 19 for a large statistical cable sample [72].

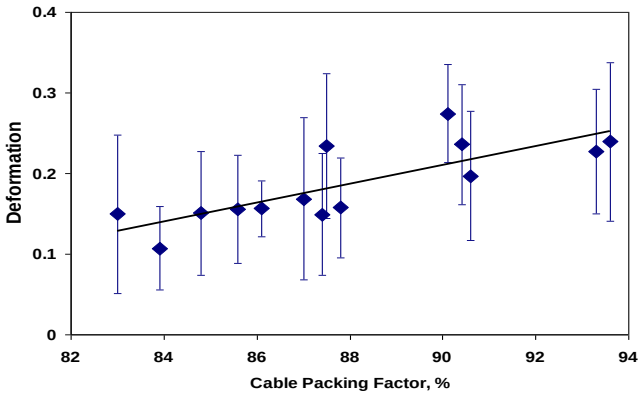

Fig. 19. Average strand deformation as a function of cable *PF* for a large number of cables. Error bars represent the standard deviation of the deformation distribution [72].

Fig. 20 (bottom), where the deformation of each strand in a keystoned and rectangular cable is plotted as function of its position in the cable [71, 72], shows what happens locally in each strand. A schematic of strand location is in Fig. 21 (top). In both cables in Figure the largest deformation values are found in the stands at both cable edges. The average strand deformation is lower in the least compacted cable.

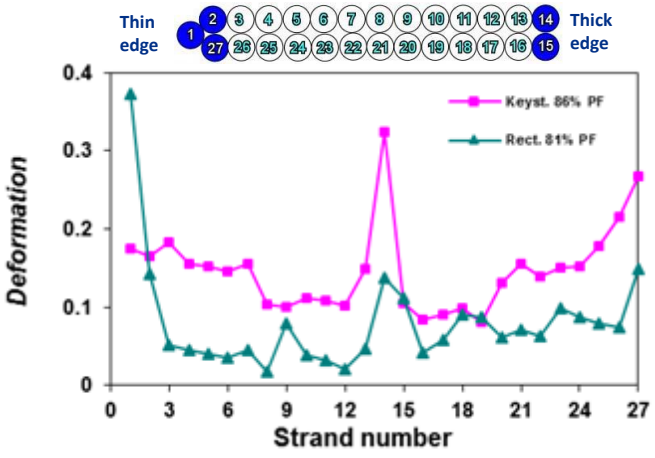

Fig. 20. Strand deformation as a function of position in 27-strand cable (bottom). A schematic of the strand locations is shown at the top [72].

Subelement plastic deformation. Similarly to the empirical formula used for strand deformation ε_{str}, subelement plastic deformation ε_{SE} could be defined as follows:

$$\varepsilon_{SE} = \frac{d_{max} - d_{min}}{d_0},$$

where d_{max} and d_{min} are the longest and shortest diameters measured through the subelement center, and d_0 is the original round subelement size.

Fig. 21 shows measured distributions of subelement d_{max} in round strands and in strands extracted from cables with different *PF*s. The increase of the subelement size after cabling, as well as their possible mechanical merging and electromagnetic coupling observed in some cases [73], provide significant impact on a magnet quench performance, due to large local flux jumps instabilities.

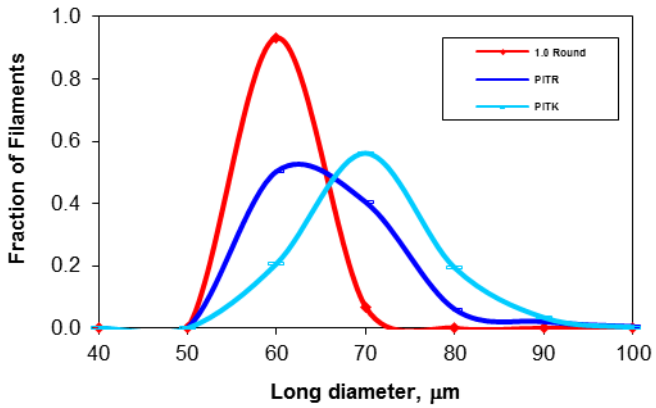

Fig. 21. Distributions of subelement largest dimension in round and extracted strands with different cable *PF*'s [72].

The effects of cable width deformation on subelement plastic deformation were also simulated using a Finite Element Model [74]. The equivalent plastic strain distribution, shown in Fig. 22 for the edge strand, is a good predictor of damage. These simulations also show that in a cable the largest values of plastic subelement deformation are generally located in the innermost part of the edge strand. These maximum values are plotted in Fig. 23 as function of width deformation R_w. A conclusion from these studies was that exceedingly compacting the cable in width produces a rapid increase in strain in the innermost part of the edge strand.

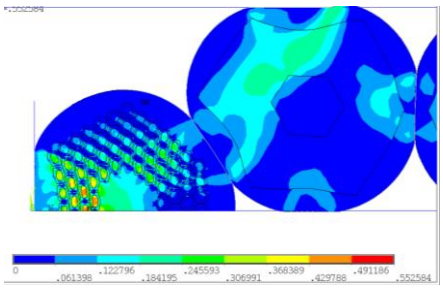

Fig. 22. Equivalent plastic strain at edge strands for a 40-strand rectangular cable having edge deformation of 0.92 and width deformation of 0.95 [74].

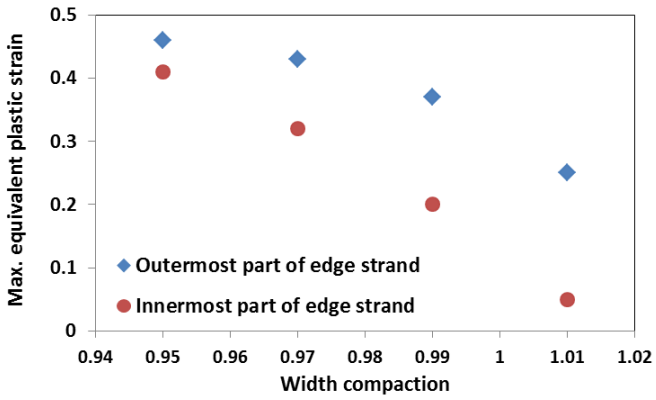

Fig. 23. Maximum equivalent plastic strain values in edge strand as function of cable width deformation for a 40-strand rectangular cable having edge compaction t_c of 0.92 [74].

Odd vs even strand number. The effect of even and odd number of strands in a cable of same cross section was evaluated in [71] using two keystoned NbTi cables with 27 and 28 strands of 1 mm in diameter. Comparison of these two cables demonstrated that, although the cable with an odd number of strands has a slightly smaller packing factor, it remained mechanically stable and had a smaller value and variation of the minor edge compaction. The analysis of subelement deformation inside strands at the cable edges demonstrated better results for the cable with odd number of strands, but more statistics would be needed to make this conclusion significant.

C. Cable Fabrication and Quality Control

Rutherford cables are produced using special cabling machines. The design features and parameters of these machines are reported elsewhere [68], [71], [75].

During cabling, attention is paid to the cable wide and narrow surfaces to exclude strand cross overs and sharp edges. The cable width and thickness are measured periodically or continuously to keep their values within the required tolerances, which are usually of ±6 μm for thickness and of ±24 μm for width. Typical variations of nominal cable width and thickness along the cable length during cable fabrication are plotted in Fig. 24.

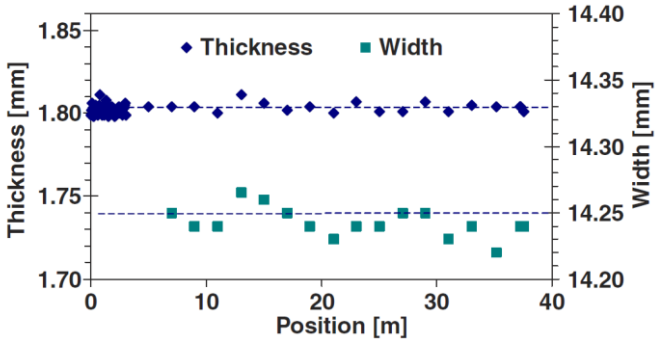

Fig. 24. Typical variations of cable width and thickness along the length of a keystoned cable: width = 14.243± 0.011 mm, thickness = 1.802 ± 0.003 mm.

D. Cable Size Change After Reaction

It is known that Nb-Sn composite strands expand after reaction due to formation of the Nb_3Sn A15 phase. Whereas in round strands this expansion is isotropic, an anisotropic volume expansion was observed for Nb_3Sn Rutherford cables [76]. While the cable width did not change significantly, the thickness increased by more than expected. To check the hypothesis that the plastic deformation imparted during cabling would release itself through heat treatment, Nb_3Sn strands of different technologies were flat-rolled down to various sizes. The thickness expansion was always larger than the width expansion for both strands and cables. Furthermore, the amount of volume expansion appeared to depend on the strand technology and to be a function of the Nb-Sn content.

The change in dimensions before and after reaction was more recently measured for keystoned cables based on state-of-the-art RRP® strands used in 11 T dipoles [66] and LARP quadrupole models [77]. The average width expansion was 2.6%, the average mid-thickness expansion was 3.9%, and the average length decrease was 0.3%. Some typical LARP cables were reacted under two different conditions: "unconfined" and "confined." In the first case, the cable is left free to expand or contract in all directions. In the "confined" case, the cable is locked transversally but allowed to freely expand longitudinally. Unlike the individual strands, the "unconfined" cable tests showed a clear longitudinal contraction. The 2-pass cables contracted by about 0.1 to 0.2% whereas the 1-pass cables by about 0.2 to 0.3%. The thickness and the width increased by 1.4% to 4% and by 1.5% to 2% respectively, without any definite correlation to the way the cable was fabricated. When "confined", the cables elongated about 0.4% and the thickness increased by about 2%. The width does not change due to the nature of the confinement.

For the purpose of magnetic design optimization, it is the reacted thickness and width values which need to be included in the cable dimensions. The coil dimensions in the winding and curing tooling are determined by the unreacted cable cross section, whereas the coil dimensions in the reaction and impregnation tooling are based on the reacted cable cross section.

V. Nb_3Sn Rutherford Cables Properties

In this section, we detail those key research activities and methods used in the International community that helped study and solve most of the aspects required of Nb_3Sn cables for magnet realization. This includes I_c measurements at high and low fields, flux jump instabilities, effect of cabling deformation on I_c, J_A, *RRR* and stability, effect of transverse pressure on I_c, and interstrand contact resistance.

A. Cable I_c Measurements

I_c evaluation of Rutherford cables is performed by either testing short cables samples or individually extracted strands. The good correlation of cable and extracted strand test results, as shown for instance in Fig. 25, confirms the validity of both approaches. The keystoned cable sample, whose results are shown in Figure, was made of 40 RRP® Nb_3Sn strands and was heat treated together with witness samples of its extracted strands. Closed symbols represent I_c data measured in a smooth voltage-current transition, whereas open symbols denote the maximum current I_q as reached before an abrupt quench due to instabilities. Self-field corrections were applied in this plot to both cable and strand test results. A good correlation between extracted strand and cable test results demonstrates the small variation of strand properties within billets that are used, and confirms a uniform transport current distribution during a cable test.

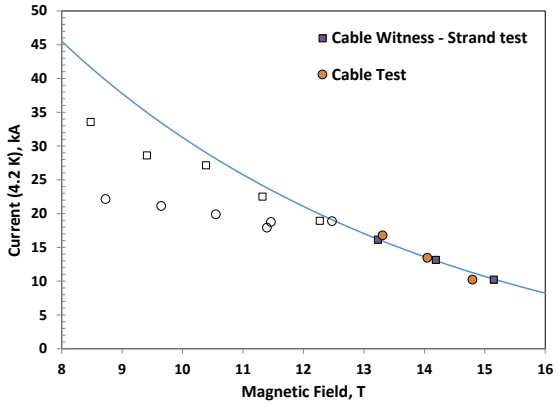

Fig. 25. Cable quench current vs. magnetic field for an insulated Nb_3Sn cable sample made of 40 RRP® Nb_3Sn strands [52].

B. Flux Jump Instabilities in Cables

Flux jump instabilities observed in Nb_3Sn strands were studied also in cable short samples. Cable samples made of different Nb_3Sn strands were tested at Fermilab in self-field at T=2 to 4.3K using a 28 kA SC transformer [78], at BNL in external magnetic fields up to 7 T at 4.3K, and at CERN in external magnetic fields up to 10 T and T=1.8 to 4.2 K [79]. The results of testing 28-strand MJR and PIT cable samples at BNL, CERN and Fermilab at 4.3 K are presented in Fig. 26 [80]. There is an excellent correlation of experimental data for similar samples tested at the three different test facilities.

Analysis and comparison of flux jump instabilities in Rutherford cables and corresponding round wires show that these instabilities are larger in cables than in round wires due to subelement deformations and possible merging, which lead to an increase of $d_{eff.}$.

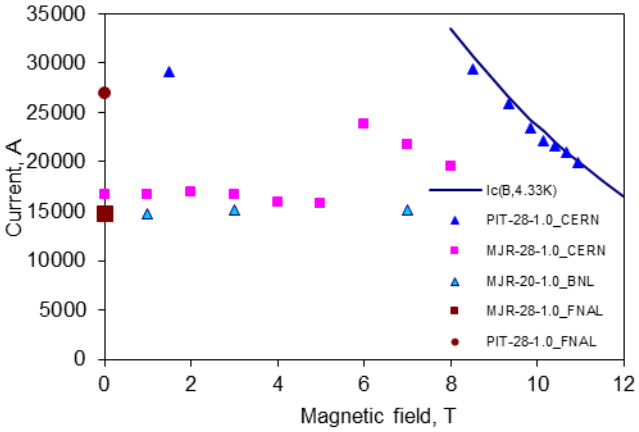

Fig. 26. 28-strand MJR and PIT cable samples tested at BNL, CERN and FNAL [80].

C. *Effect of Cable Plastic Deformation*

The effect of cable plastic deformation on the critical current I_c, average critical current density J_A, minimal stability curent I_s and matrix *RRR* was studied using extracted strands [81]. The results of I_c measurements made on extracted strands were compared with those made on round strands used in cables. The average cable J_A at 4.2 K and 12 T normalized to the average J_A of a cable made of undeformed round strands (*PF* = 78.5%) is plotted in Fig. 27 (top) as a function of cable *PF*. Some early IT strands demonstrated relative I_c degradation up to 80% at *PF*s above 84%. A large I_c degradation was also observed in early PIT strands [81]. However, after strand optimization, in particular by increasing the subelement spacing in RRP® strands and by using round filaments in PIT strands, the I_c degradation was reduced to 15% or less at *PF*s up to 94%. At a *PF* between 84 and 87%, which is typical for Nb_3Sn Rutherford cables, the I_c degradation in well optimized cables is usually ~5% or less.

Fig. 27 (bottom) shows the normalized average critical current density J_A as function of cable *PF*. It can be seen from both plots in Figure that for all Nb_3Sn strand technologies, the average J_A has an almost flat behavior with *PF* and is larger than in the undeformed cable when the I_c degradation is less than the reduction of cable cross section. Similar measurements performed on cables made with modern RRP® and PIT strands are consistent with these data.

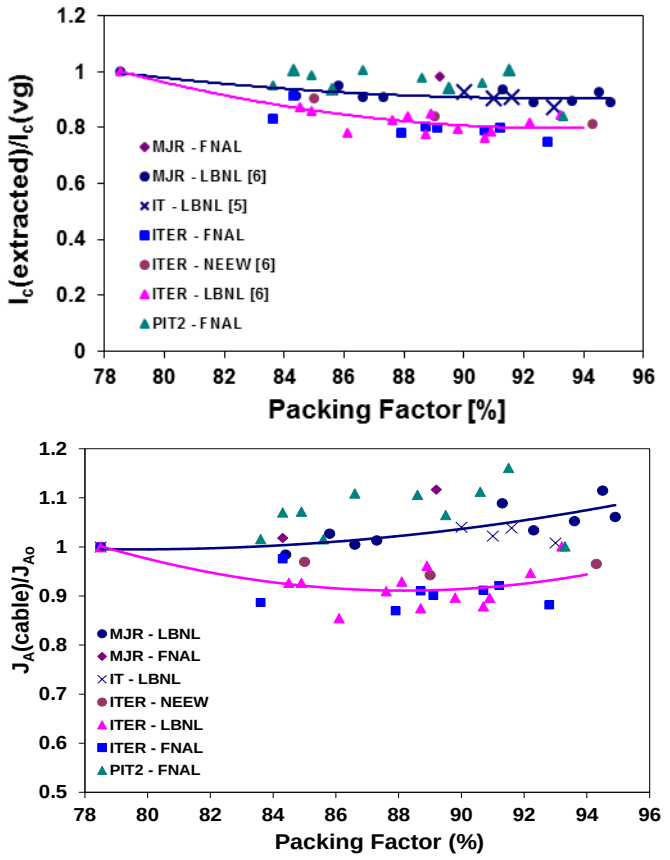

Fig. 27. Normalized cable I_c (top) and average J_A (bottom) at 4.2 K and 12 T as a function of *PF* for cables made with IT, MJR and PIT Nb_3Sn strands [81].

It was found that the effect of cabling on the stability current I_S and on the *RRR* is however much stronger than on the I_c, and that subelement damage in a cable is best seen through I_S degradation of its extracted strands [82]. This was confirmed by a cabling study [72] performed to compare the behavior in keystoned cables over an ample *PF* range of an RRP® strand with 50% increased Cu spacing between subelements (called RRP1 in Figures) with respect to the standard RRP® wire (called RRP2 in Figures). The I_s at 4.2 K and the *RRR* vs. cable *PF* are plotted in Figs. 28 and 29. The I_S and *RRR* measured values of extracted strands are not as reproducible as in round strands. However, it was shown that the RRP® strand with extra spacing between subelements was able to maintain a higher I_S in the higher *PF* range (above 90%). This indicated that using the improved conductors affords more flexibility for cables more ideal to magnet technology, for which larger keystone angles and larger average cable J_A's are desirable.

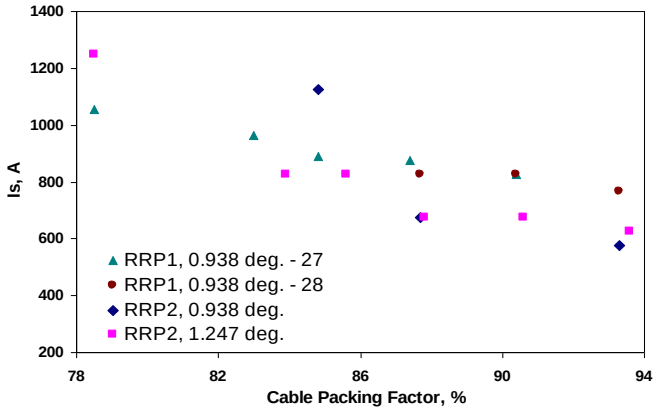

Fig. 28. I_S at 4.2 K as a function of cable packing factor for RRP® strands. RRP1 in legend represents a wire with 50% increased Cu spacing between subelements with respect to a standard RRP® wire called RRP2 [72].

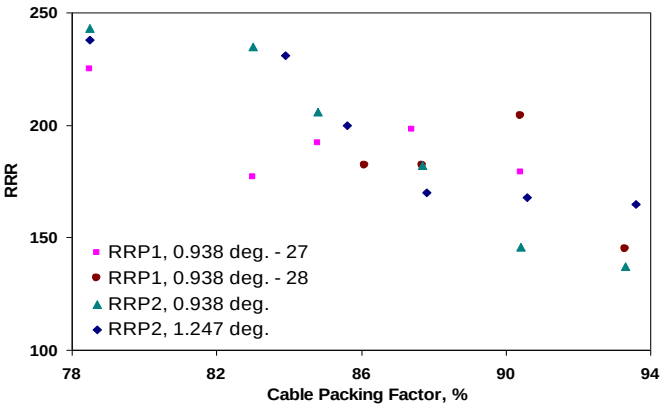

Fig. 29. *RRR* as a function of cable packing factor for RRP® strands. RRP1 in legend represents a wire with 50% increased Cu spacing between subelements with respect to a standard RRP® wire called RRP2 [72].

Based on the results of I_c degradation in Nb_3Sn Rutherford cables, high values of *PF* of 92 to 95% provide the highest J_A. However, large I_s and *RRR* degradation due to large deformations and possible damage and merging of the delicate subelements impose an optimal *PF* within 84 to 87%.

D. RRR Variation Along a Strand

Due to the larger strand deformation at the cable edges, it was expected that *RRR* varied along a strand. Longitudinal variations of *RRR* were estimated from multiple-tap measurements along the length of strands extracted from cables [83]. Voltage taps were placed across straight sections and across the bends of extracted strands (Fig. 30). Resistivity measurements made on extracted strands showed significant *RRR* degradation from the *RRR* ≈ 116±17 for strand segments on the cable faces. On the edges the results were an order of magnitude smaller, *RRR* ≈ 13±5, consistently with local Sn leakages through the diffusion barriers caused by the strong deformation at the cable edges. The average value obtained for a strand when using voltage taps far apart is still large 81±21, due to the localization of the highly deformed edge region. Cables with lesser degradation have been fabricated. However, such large *RRR* degradation at the edges is often found even in cables with low packing factors, and does not seem particularly sensitive to details of edge compaction.

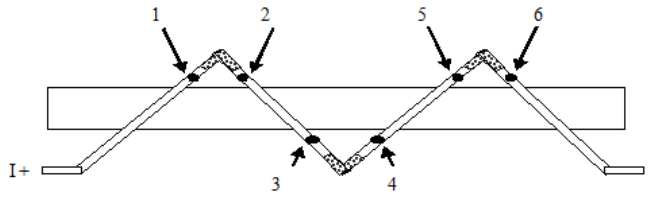

Fig. 30. *RRR* sample configuration. Points 1-6 are voltage taps, I+ and I- are the current leads. Measurements taken between 1-2, 3-4, and 5-6 measure *RRR* as the strand bend over the cable edges, while measurements between 2-3 and 4-5 measure the "straight" sections of the strand on the cable faces [83].

E. Effect of Transverse Pressure

Transverse stress is the largest stress component in accelerator magnets up to high magnetic fields. Studies were performed by applying pressure to impregnated cable samples and testing individual strands inside the cable structure [84-88]. Fig. 31 shows the I_c sensitivity of IT, PIT and RRP® strands to transverse pressures up to 210 MPa [87]. It was found that cables made of PIT strands are more sensitive to transverse pressure than cables made with IT strands. It should be noted that these data represent the effect of uni-axial and not multi-axial strain, since the experimental setup allows for the sample to expand laterally. This produces larger strain values on the cable sample than for instance on a laterally constrained one, and therefore these are conservative results.

At CERN a transverse pressure measurement was performed at 4.3 K on a 10 mm wide Rutherford cable made of eighteen 1 mm Nb_3Sn PIT strands [88]. The setup that was used is made to laterally constrain the sample. With a peak field of about 11.6 T and a transversal load of approximately 155 MPa, the quench current had a reduction of only 24%. The discrepancy with the above results can be explained with the different strain conditions seen by samples in the two experimental configurations. In [88], the setup reproduces the uni-axial load case A, represented in Fig. 32 (left), which has $\sigma_{yy} = -p$ and $\sigma_{xx} = \sigma_{zz} = 0$. The second load case, multi-axial case B, represented in Fig. 31 (right), has $\sigma_{yy} = -p$, $\sigma_{xx} = -\nu p$ and $\sigma_{zz} = 0$.

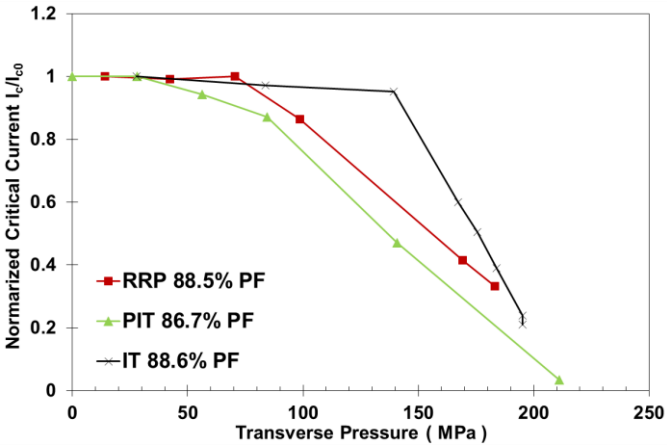

Fig. 31. Normalized I_c(4.2K,12T) vs. uni-axial transverse pressure on Rutherford cable face for a number of Nb_3Sn conductors [87].

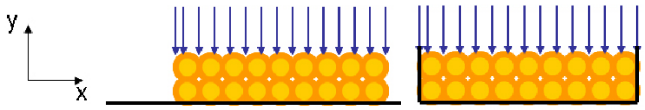

Fig. 32. Uni-axial case A, free sides (left), and multi-axial case B (right).

Whichever equivalent stress or strain model is used, it is striaghtforward to verify that load case A always sees strain values larger or at best equal to those produced in load case B. Needless to say that in magnets the strain distribution is very complex and it is therefore safe to assume that the uni-axial load case produces conservative estimates of I_c sensitivity.

F. Interstrand Resistance

Direct measurements of R_c and R_a contact resistances performed under transverse pressure in [89] gave R_c=1.1 to 1.4 μΩ and R_a=8 to 16 μΩ (10 to 100 MPa) for uncored cables, and R_c=150 to 275 μΩ and R_a=1.5 to 1.9 μΩ (10 to 100 MPa) for cables with a 0.025 mm stainless steel (SS) core. For comparison, in LHC NbTi cables R_c is about 10 to 20 μΩ [90], which is more than 10 times larger than in a Nb_3Sn cable without a resistive core and more than a order of magnitude lower than in a Nb_3Sn cable with resistive core.

Similarly low R_c values of ~0.1 to 0.4 μΩ, measured in Nb_3Sn Rutherford cables reacted in coil under pressure, are reported in [91]-[95]. In cables with a full-width SS core, an excessively high R_c of 246 μΩ was measured. The contact resistances in cable samples were determined based on AC loss measurements.

A special technique to measure interstrand contact resistances in magnet coils was developed at FNAL [96]. The results of measurements in pole and midplane turns of a dipole coil have shown that the adjacent contact resistances were uniform in azimuthal and radial directions, and quite low, R_a from 0.8 to 4.3 μΩ, providing good conditions for current sharing in the cable. The range of crossover resistances R_c and variations in the azimuthal direction were instead rather large. R_c changed from 4.4 to 4.5 μΩ in pole turns to 20 to 30 and higher in the midplane turns of both layers.

Studies of interstrand contact resistances in Nb_3Sn Rutherford cables have shown that using SS core is very

efficient in reducing the level of eddy current effects (magnetization, AC loss) in cables. It also helps to reduce the observed variations of contact resistances in Nb_3Sn coils.

VI. Next Steps and R&D Goals

State of the art Nb_3Sn strands and Rutherford cables allow accelerator magnets with nominal operation fields of 10 to 11 T and up to 20% field margin for reliable operation in accelerators. The first Nb_3Sn 11 T dipoles and 150 mm aperture quadrupoles are planned to be installed in the LHC to improve the machine collimation system and achieve higher luminosity [97]. The new post-LHC hadron colliders, whose feasibility studies have started recently in US, EU and China, need more powerful magnets with nominal operation fields ~15 to 16 T [98] and up to 20% margin, bringing the design field to the level of 18 to 19 T.

The maximum design field B_{max} in accelerator magnets is proportional to the critical current density J_c at B_{max} and to the coil width w:

$$B_{max} \sim J_c(B_{max}) \cdot w.$$

Based on this formula, higher fields in accelerator magnets can be achieved by using materials with higher J_c and/or wider coils. Each option has limitations to be taken into consideration, such as higher stress level and storage energy, superconductor and magnet cost, etc.

Target parameters for the next generation accelerator magnets with B_{op}~15 to 16 T are under discussion. Below we describe some R&D directions which are important to achieve target fields of 15 to 16 T with the required margin.

A. Critical Current Density

With the present level of J_c of ~2.5 to 3 kA/mm^2 at 12 T and 4.2 K, a 16 T design field requires a coil width of ~60 mm. For a design field of 18 to 19 T to provide margin during operation at 15 to 16 T would require a coil thickness increased to 150 mm at least. To reduce the coil volume (i.e. magnet cost), 3 T margin could be provided by increasing the J_c in 60 mm wide coils to 3.7 kA/mm^2 at 12T or to 1.8 kA/mm^2 at 15 T. It is thought that this modest J_c increase can be achieved by further optimization of subelement architecture and Sn content, and by improving its diffusion to the periferal Nb filaments inside the subelements.

More substantial improvements of Nb_3Sn J_c at high fields, by a factor of 2 or more, would also be desirable to increase reliability and reduce the accelerator magnet cost. This will require significant enhancement of pinning in Nb_3Sn commercial wires. For instance [47] predicts that the J_c(12T, 4.2K) of Nb_3Sn could be improved by a factor of 4 to 5 by increasing the transverse flux pinning contribution (typical of NbTi) with respect to the longitudinal one that prevails in current Nb_3Sn materials. This would however require nano-engineering of the material and large effort investments. Another well-known method to improve J_c in Nb_3Sn is by enhancement of the pinning centers density through grain refinement or by the inclusion of engineered pinning centers. Both these options, though demonstrated on laboratory samples [99], [100], have yet to be validated in commercial wires.

B. Strand Diameter

The larger coil width in the 15 T class magnets of 50 to 60 mm aperture requires more layers and more turns, and thus leads to larger inductance. The increase of cable width with the present strand diameter of 0.7 to 1.0 mm is restricted by the cable mechanical stability, which significantly reduces with further increases of the cable aspect ratio. The opposing needs of cable width and mechanical stability can be resolved by using strands with larger diameter. Strands with D=1.2 to 1.8 mm are needed for stable cables with aspect ratios of 17 to 12. Possible restrictions on strand diameter from self-field stability criteria, as well as difficulties with higher cable bending rigidity, could be resolved by using 6-around-1 strand cables based on 0.5 to 0.6 mm Nb_3Sn composite wires. This approach also allows optimizing the Cu cross section area by combining Nb_3Sn and pure Cu wires. A drawback is the reduction of cable packing factor.

C. Subelement Size

The increase of J_c in new strands, required to achieve higher target fields, is a strong incentive to keep d_{eff} under control to avoid premature quenches, field quality degradation at injection, field harmonics fluctuations, and voltage spikes. A d_{eff} of 40 μm or less is still a sound objective. In larger diameter strands it will lead to new strand architectures with larger number of subelements.

D. Cu Stabilizer

To provide reliable protection during a quench, 15 T magnets may need a larger cross section of Cu stabilizer. Increasing the Cu cross section in a composite Nb_3Sn wire may be limited by the wire design and fabrication process. It is also considered as a more expensive approach than adding Cu to the cable cross section. Several options have been proposed and studied [101]-[103]. R&D of large Nb_3Sn cables with large Cu fraction needs to continue.

E. RRR

The *RRR* of the Cu stabilizer is an important parameter for conductor, cable and magnet stability as well as for cable and magnet processing control. Since magnetic field and cabling significantly reduce the Cu matrix *RRR*, wire stability has to be provided by small d_{eff}. On the basis on its sensitivity to deformation, *RRR* should be mostly used as a quality control parameter during cable and magnet processing.

VII. Summary

High-performance composite wires and Rutherford cables are key components of superconducting accelerator magnets that have been pushing the frontier of particle physics in the past 30 years. While consumption is still largely dominated by the widespread use of NbTi, literally the workhorse for all HEP applications to date, we anticipate that the next five years will be decisive for Nb_3Sn. Decades of preparation have resulted in Nb_3Sn wires and cables that are approaching the necessary maturity for HEP applications. The advances in Nb_3Sn wire and Rutherford cable technologies during the past decade make it possible for the first time to consider Nb_3Sn

accelerator magnets with nominal fields up to 12 T in present, e.g. the planned LHC upgrades, and future machines.

This work will continue to achieve the limits of the Nb_3Sn technology. The main goal of Nb_3Sn superconducting wire and cable R&D programs is to understand and improve scientific and engineering aspects of Nb_3Sn strands and cables that are used to make accelerator magnets. The outcome of this effort provides conductor specifications and essential engineering data for design and construction of accelerator magnets. Coordination with industry has been and remains critical to improve performance of commercial Nb_3Sn strands and cables, and International collaboration between laboratories and universities has provided fundamental understanding at all levels.

REFERENCES

Section I

[1] http://www.superconductors.org

[2] *Superconductor Material Science*, S. Foner, B. B. Schwartz, Plenum Press, N. Y., (1981).

[3] B. T. Matthias, T. H. Geballe, S. Geller, and E. Corenzwit, Phys. Rev. 95, 1435 (1954).

[4] J. E. Kunzler, E. Buehler, F. S. L. Hsu and J. H. Wernick, Phys. Rev. Lett. 6, 89 (1961).

[5] K. Tachikawa and Y. Tanaka, Japan. J. Appl. Phys. 5, 834 (1966).

[6] A. R. Kaufman and J. J. Pickett, Bull. Am. Phys. Soc. 15, 833 (1970).

[7] K. Tachikawa, Int. Cryo. Engin. Conf., Berlin (1970); Iliffle Sci. Tech. Pub. 339 (1971).

[8] N. Mitchell et al., "Conductor designs for the ITER toroidal and poloidal magnet systems," IEEE Trans. on Mag., 1994, p. 1602.

[9] J. A. Parrell, M. B. Field, Y. Zhang, and S. Hong, Adv. Cryo. Eng. (Materials) 50B, 369 (2004).

[10] J. H. Lindenhovius, E.M. Hornsveld, A.den Ouden, W.A.J. Wessel, and H.H.J. ten Kate, Progress in the Development of Nb_3Sn Conductors based on the "Powder in Tube" Method with Finer Filaments, IEEE Trans. on Applied Superconductivity 9, 1451 (1999).

[11] A. Godeke, A. den Ouden, A. Nijhuis, and H. H. J. ten Kate, Cryogenics 48, 308 (2008).

[12] A. Godeke, "A review of the properties of Nb_3Sn and their variation with A15 composition, morphology and strain state", Supercond. Sci. Technol. 19 (2006) R68–R80.

[13] D. R. Dietderich, A. Godeke, "Nb_3Sn research and development in the USA – Wires and cables", Cryogenics 48, 331 (2008).

[14] L. Bottura and A. Godeke, "Superconducting materials and conductors, fabrication, and limiting parameters," Reviews of Accelerator Science and Technology, 5 (2012), p. 25.

[15] M. N. Wilson, "Superconducting Magnets for Accelerators: a Review," IEEE Trans. on Appl. Supercond., Vol. 7, No. 2, June 1997, p. 727.

[16] G. Gallagher-Daggit, Superconductor cables for pulsed dipole magnets. Technical report (Rutherford Laboratory Memorandum No. RHEL/M/A25, 1973).

[17] S. A. Gourlay, "High Field Magnet R&D in the USA," IEEE Trans. on Appl. Supercond., Vol. 14, No.2, June 2004, p.333.

[18] A. Devred et al., "High field accelerator magnet R&D in Europe," IEEE Trans. Appl. Supercond., vol. 14, no. 2, pp. 339–344, 2004.

Section II

[19] M. N. Wilson, Superconducting Magnets, Oxford University Press, New York, 1983.

[20] Y. Hashimoto, K. Yoshizaki, and M. Tanaka, Proc. of 5th Internat. Cryo. Eng. Conf., Kyoto, Japan (1974), p. 332.

[21] S. Mattafirri et al., "Kinetics of Phase Growth in the Cu-Sn System and Application to Composite Nb_3Sn Strands", IEEE Trans. Appl. Sup., V. 13, No. 2, p. 3418 (2003).

[22] J.-M. Rey et al., "Effect of Partially Reacting Nb_3Sn Before Magnet Winding on the Strand Critical Current", Advances in Cryogenic Engineering, V. 48, AIP, V. 614, pp. 1001-1007 (2002).

[23] L.T. Summers et al., "A model for the prediction of Nb_3Sn critical current as a function of field, temperature, strain and radiation damage", IEEE Trans. Magn., 27 (2): 2041-2044 (1991).

[24] J.W. Ekin, "Experimental Techniques for Low-Temperature Measurements", OXFORD University Press, pp. 461-463.

[25] V.V. Kashikhin and A.V. Zlobin, "Correction of the Persistent Current Effect in Nb_3Sn Dipole Magnets", IEEE Transactions on Applied Superconductivity, v. 11, No. 1, March 2001, p. 2058.

[26] W. J. Carr, J. Appl. Phys., 45, 1974, p.935.

[27] L.D. Cooley, A.K. Ghosh and R.M. Scanlan, "Costs of high-field superconducting strands for particle accelerator magnets", Supercond. Sci. Technol. 18 (2005) R51–R65.

[28] R. M. Scanlan, "Conductor Development for High Energy Physics-Plans and Status of the U. S. Program", IEEE Trans. on Applied Superconductivity, vol. 11, No. 1, March 2001, p. 2150.

[29] R. M. Scanlan, D.R. Dietderich, "Progress and Plans for the U.S. HEP Conductor Development Program", IEEE Trans. on Applied Superconductivity, vol. 13, No. 2, June 2003, p. 1536.

[30] G. J. Peters et al., "The DOE High Energy Physics SBIR/STTR Superconductivity Program", IEEE Trans. on Applied Superconductivity, vol. 13, No. 2, June 2003, p. 1520.

[31] M. Durante et al., "Development of a Nb_3Sn multifilamentary wire for accelerator magnet applications," Physica C, vol. 354, pp. 449–453, 2001.

[32] J. L. H. Lindenhovius et al., "Powder-in-tube (PIT) Nb_3Sn conductors for high field magnets," IEEE Trans. Appl. Supercond., vol. 10, no. 1, pp. 975–978, March 2000.

[33] M. Wake et al., "Development of high current density Nb_3Sn conductor with distributed tin configuration," Adv. Cryo. Eng., vol. 50B, pp. 410–416, 2004.

[34] D.R. Dietderich, A. Godeke, "Nb_3Sn research and development in the USA – Wires and cables", Cryogenics 48, 331 (2008).

[35] M.B. Field et al. "Optimizing Nb_3Sn Conductors for High Field Applications," IEEE Trans. on Applied Superconductivity, Vol. 24, No. 3, June 2014, 6001105.

Section III

[36] R.M. Scanlan, W.A. Fietz, and E.F. Koch, J. Appl. Phys. 46, 2244 (1975).

[37] C.S. Pande and M. Suenaga, Appl. Phys. Letters 29, 443 (1976).

[38] A.W. West and R.D. Rawlings, J. Mater. Sci. 12, 1862 (1977),.

[39] P.E. Madsen and R.F. Hills, IEEE Trans. on Magnetics MAG-15, 181 (1979).

[40] D. Dew-Hughes, *Phil. Mag. B*, vol. 55, No. 4, pp. 459-479, 1987.

[41] E. J. Kramer, *J. Appl. Phys*., vol. 44, No. 3, pp. 1360-70, March 1973.

[42] M. Suenaga, K. Tsuchiya, N. Higuchi, and K. Tachikawa, *Cryogenics*, vol. 25, pp. 123-8, 1985.

[43] J. E. Evetts and C. J. Plummer, *Proc. Int. Symp. on Flux Pinning and Electromagnetic Properties in Superconductors,* edited by T. Matsushita, K. Yamafuji, and F. Irie, Fukuoka: Matsukuma, 1985, p. 146.

[44] D. F. Hampshire, H. Jones, and E. W. J. Mitchell, *IEEE Trans. Mag.*, vol. 21, pp. 289-92, 1985.

[45] W. Schauer, and W. Schelb, *IEEE Trans. Mag.*, vol. 17, pp. 374-377, 1981.

[46] R. Taillard and A. Ustinov, "Evolutions of grains during the heat treatments of internal-tin Nb_3Sn," *Adv. Cry. Eng.*, vol. 46B, 2000.

[47] J. McDonald et al., "A Model for J_c in Granular A-15 Superconductors", IEEE Trans. Appl. Sup., V. 11, No. 1, p. 3884 (2001).

[48] E. Barzi et al., "Nb_3Sn Phase Growth and Superconducting Properties during Heat Treatment", IEEE Trans. Appl. Sup., V. 13, No. 2, p. 3414 (2003).

[49] A. K. Ghosh, L. D. Cooley, and A. R. Moodenbaugh, "Investigation of instability in high J_c Nb_3Sn strands," IEEE Trans. Appl. Supercond., vol. 15, no. 2, pp. 3360–3363, Jun. 2005.

[50] Lim K C, Thomson J D, and Webb G W. "Electronic density of states and T_c in Nb_3Sn under pressure", Phys Rev B 1983; 27: 2781-2787.

[51] Li Qiao, Lin Yang and Jie Song, CRYOGENICS-D-14-00136R1 (2015).

[52] E. Barzi, D. Turrioni, and A.V. Zlobin, "Progress in Nb_3Sn RRP Strand Studies and Rutherford Cable Development at FNAL", IEEE Trans. on Appl. Supercond., Vol. 24, Issue 3, June 2014 Page 6000808.

[53] Cheggour N et al., Supercond. Sci. Technol. 23 (2010) 052002.

[54] G. Ambrosio et al., “Study of the React and Wind Technique for a Nb_3Sn Common Coil Dipole”, IEEE Trans. Appl. Sup., V. 10, No. 1, p. 338 (2000).
[55] G. Ambrosio et al., “Development of React & Wind Common Coil Dipoles for VLHC”, IEEE Trans. Appl. Sup., V. 11, No. 1, p. 2172 (2001).
[56] P. Bauer et al., “Fabrication and Testing of Rutherford-type Cables for React and Wind Accelerator Magnets”, IEEE Trans. Appl. Sup., V. 11, No. 1, p. 2457 (2001).
[57] H. Brechna, Superconducting magnet systems, Springer, Berlin, 1973.
[58] E. Barzi, “Superconductor and Cable R&D for High Field Accelerator Magnets at Fermilab”, Progress of Nb-Based Superconductors, printed Feb. 18, 2005, by Maeda printing Co., LTD, Editors K. Inoue, T. Takeuchi, A. Kikuchi.
[59] R. Hancox, “Enthalpy Stabilized Superconducting Magnets,” IEEE Trans. on Magnetics, Vol. MAG-4, Issue 3, September 1968, p. 486.
[60] V.V. Kashikhin, A.V. Zlobin, “Magnetic Instabilities in Nb_3Sn Strands and Cables”, IEEE Trans. on Appl. Supercond., Vol. 15, Issue 2, June 2005, p. 1621.
[61] M. D. Sumption and E. W. Collings, “Modeling current-field instability in high performance Nb_3Sn strands in moderate field,” IEEE Trans. Appl. Supercond., vol. 17, pp. 2714–2717, 2007.
[62] B. Bordini et al., “Self-field effects in magneto-thermal instabilities for Nb-Sn strands,” IEEE Trans. Appl. Supercond., vol. 18, p. 1309, 2008.
[63] A.V. Zlobin, V.V. Kashikhin, E. Barzi, “Effect of Magnetic Instabilities in Superconductor on Nb_3Sn Accelerator Magnet Performance”, IEEE Trans. on Applied Superconductivity, Vol. 16, Issue 2, June 2006 p. 1308.
[64] A.K. Ghosh et al., “Investigation of Instability in High J_c Nb_3Sn Strands,” IEEE Trans. on Appl. Supercond., Vol. 15, Issue 2, June 2005, p. 3360.
[65] B. Bordini et al., "Impact of the Residual Resistivity Ratio on the Stability of Nb_3Sn Magnets", IEEE Ttans. on Appl. Sup., Vol. 22, No. 3, June 2012, 4705804.

Section IV

[66] E. Barzi et al., “Development and Fabrication of Nb_3Sn Rutherford Cable for the 11 T DS Dipole Demonstration Model”, IEEE Transactions on Applied Superconductivity, Vol. 22, Issue 3, June 2012 6000805.
[67] M.N. Wilson, Preprint RHEL/M/A26, 1972.
[68] J.D. Adams et al., “Rutherford Cables with Anisotropic Transverse Resistance”, IEEE Trans. on Magnetics, Vol. 7, No. 2, June 1997, p. 958.
[69] V.E. Sytnikov, et al., "Coupling current losses in superconducting transposed conductors located in changing magnetic fields," Cryogenics, 2 9, pp. 926-930, 1989.
[70] A. Devred et al., “Interstrand Resistance Measurements on Nb_3Sn Rutherford-Type Cables”, IEEE Trans. on Magnetics, Vol. 9, No. 2, June 1999, p. 722.
[71] N. Andreev et al., “Development of Rutherford-type Cables for High Field Accelerator Magnets at Fermilab”, IEEE Transactions on Applied Superconductivity, Volume 17, Issue 2, June 2007 Page(s):1027-1030.
[72] D. Turrioni, et al., “Effects of Rutherford Cable Parameters on Nb_3Sn Extracted Strand Deformation and Performance”, IEEE Transactions on Applied Superconductivity, Vol. 18, Issue 2, June 2008, p. 1114.
[73] A. Polyanskii, et al., “Evidence for Highly Localized Damage in Internal Tin and Powder-In-Tube Nb_3Sn Strands Rolled Before Reaction Obtained from Coupled Magneto-Optical Imaging and Confocal Laser Scanning Microscope”, Supercond. Sci. Technol. 22 (2009).
[74] E. Barzi, G. Gallo, and P. Neri, “FEM Analysis of Nb-Sn Rutherford-type Cables”, IEEE Trans. Appl. Sup., Vol. 22, Issue 3, June 2012.
[75] J. Grisel et al., “A unique cabling machine designed to produce Rutherford-type superconducting cable for the SSC project,” IEEE Trans. on Magnetics, Vol. 25, No. 2, March 1989, p. 1608.
[76] N. Andreev *et al.*, “Volume expansion of Nb_3Sn strands and cables during heat treatment”, *Advances in Cryogenic Engineering*, V. 48, AIP, V. 614, pp. 941-948 (2002).
[77] H. Felice, et al., “Impact of Coil Compaction on Nb_3Sn LARP HQ Magnet”, IEEE Trans. on Applied Superconductivity, Vol. 22, Issue 3, June 2012. 4001904.

Section V

[78] E. Barzi, et al., ”Study of Nb_3Sn Cable Stability at Self-field Using a SC Transformer”, IEEE Transactions on Applied Superconductivity, Volume 15, Issue 2, June 2005 Page(s):1537 – 1540.
[79] G. Ambrosio, et al., “Critical Current and Instability Threshold Measurement of Nb_3Sn Cables for High Field Accelerator Magnets”, IEEE Transactions on Applied Superconductivity, Volume 15, Issue 2, June 2005 Page(s):1545 – 1549.
[80] A.V. Zlobin et al., “R&D of Nb_3Sn Accelerator Magnets at Fermilab”, IEEE Transactions on Applied Superconductivity, Vol. 15, Issue 2, June 2005, p. 1113.
[81] E. Barzi et al., “Development and study of Rutherford-type cables for high-field accelerators magnets at Fermilab”, Supercond. Sci. Technol. 17 (May 2004) S213-S216.
[82] “RRP Nb_3Sn Strand Studies for LARP”, Emanuela Barzi, Rodger Bossert, Shlomo Caspi, Dan Dietderich, Paolo Ferracin, Arup Ghosh, Daniele Turrioni, IEEE Trans. Appl. Sup., V. 17, No. 2, p. 2607 (2007).
[83] M.D. Sumption, et al., “Measurement of RRR variation in strands extracted from Nb_3Sn-type Rutherford cable”, CEC/ICMC’07, Chattanooga, TN, July 16-20 2007.
[84] J. Van Oort, et al., “The reduction of the critical current in Nb3Sn cables under transverse loads,” IEEE Trans. Appl. Supercond., vol. 3, no. 1, pp. 559–592, Mar. 1993.
[85] G. Pasztor et al., “Transverse stress effects in Nb3Sn Cables”, IEEE Trans. Appl. Supercond., vol. 30, no. 4, July 1994, p.1938.
[86] D. R. Dietderich et al., “Critical current of superconducting Rutherford cable in high magnetic fields with transverse pressure”, IEEE Trans. Appl. Sup.,V. 9, 1999, p. 122.
[87] E. Barzi, T. Wokas, A.V. Zlobin, “Sensitivity of Nb_3Sn Rutherford-type Cables to Transverse Pressure”, IEEE Transactions on Applied Superconductivity, Volume 15, Issue 2, June 2005, p. 1541.
[88] B. Bordini et al., “Critical Current Measurements of High-J_c Nb_3Sn Rutherford Cables Under Transverse Compression”, IEEE Trans. on Appl. Supercond., Vol. 24, Issue 3, June 2014 9501005
[89] Devred et al., “Interstrand Resistance Measurements on Nb_3Sn Rutherford-Type Cables”, IEEE Trans. on Magnetics, Vol. 9, No. 2, June 1999, p. 722.
[90] Z. Ang, et al., IEEE Trans. Appl. Supercond., vol. 9, pp. 735–741, 1999.
[91] E. W. Collings, et al., IEEE Trans. Appl. Supercond., vol. 20, pp. 1387–1390, 2010.
[92] M. D. Sumption, et al., IEEE Trans. Appl. Supercond., vol. 16, pp. 1200–1203, 2006.
[93] M. D. Sumption, et al., Adv. Cryo. Eng. (Materials), vol. 50, pp. 781–788, 2004.
[94] E. W. Collings, et al., IEEE Trans. Appl. Supercond., vol. 17, pp. 2494–2497, 2007.
[95] E.W. Collings et al., ”Influence of a Stainless Steel Core on Coupling Loss, Interstrand Contact Resistance, and Magnetization of an Nb_3Sn Rutherford Cable”, IEEE Transactions on Applied Superconductivity, Volume 18, Issue 2, June 2008 Page(s): 1301 - 1304
[96] G. Ambrosio et al., “Measurement of Inter-Strand Contact Resistance in Epoxy Impregnated Nb_3Sn Rutherford Cables,” CEC/ICMC2003, Alaska, September 22-25 2003.

Section VI

[97] L. Bottura et al., “Advanced Accelerator Magnets for Upgrading the LHC,” IEEE Transactions on Applied Superconductivity, vol. 22, no. 3, p. 4002008, 2012.
[98] D. Schulte et al, “Specification: Future Circular Collider Study - Hadron Collider Parameters,” EDMS No. 1342402, FCC-ACC-SPC-0001 v.1.0.dietderich, thin films with APC.
[99] D.R. Dietderich et al. “High critical current densities in Nb_3Sn films with engineered microstructures – artificial pinning microstructures”, Adv Cryo Eng (Mater) 1998;44:951.
[100] X. Xu, M.D. Sumption, X. Peng, “Internally Oxidized Nb_3Sn Strands with Fine Grain Size and High Critical Current Density”, Adv. Mater. 2014, 00, 1–4
[101] V.V. Kashikhin, A.V. Zlobin, “Single-layer high field dipole magnets”, Paper RPPH081, PAC’01, Chicago, IL, June 2001, v.5, p.3415.
[102] D. R. Chichili et al., “Fabrication of Nb_3Sn Shell-Type Coils with Pre-Preg Ceramic Insulation”, CEC/ICMC 2003, Alaska, September 22-25 2003.
[103] M. Coccoli et al., “Fabrication and Performance of Nb_3Sn Rutherford-Type Cable With Cu Added as a Separate Component,” IEEE Transactions on Applied Superconductivity, 14, 2, 2004.